ACS NANO
Cite This: ACS Nano 2019, 13, 6396–6408
www.acsnano.org

ARTICLE

Dexamethasone Increases Cisplatin-Loaded Nanocarrier Delivery and Efficacy in Metastatic Breast Cancer by Normalizing the Tumor Microenvironment

John D. Martin,[†] Myrofora Panagi,[‡] Chenyu Wang,[§] Thahomina T. Khan,[†] Margaret R. Martin,[†] Chrysovalantis Voutouri,[‡] Kazuko Toh,[∥] Panagiotis Papageorgis,[‡,⊥] Fotios Mpekris,[‡] Christiana Polydorou,[‡] Genichiro Ishii,[#] Shinichiro Takahashi,[¶] Naoto Gotohda,[¶] Toshiyuki Suzuki,[¶] Matthew E. Wilhelm,[§] Vinicio Alejandro Melo,[∥] Sabina Quader,[∥] Jumpei Norimatsu,[†] Ryan M. Lanning,[$] Motohiro Kojima,[#] Matthew David Stuber,[§] Triantafyllos Stylianopoulos,[‡] Kazunori Kataoka,[*,∥,△] and Horacio Cabral[*,†]

[†]Department of Bioengineering, Graduate School of Engineering, The University of Tokyo, Bunkyo, Tokyo 113-8656, Japan
[‡]Cancer Biophysics Laboratory, Department of Mechanical and Manufacturing Engineering, University of Cyprus, Nicosia 1678, Cyprus
[§]Process Systems and Operations Research Laboratory, Department of Chemical and Biomolecular Engineering, University of Connecticut, Storrs, Connecticut 06269, United States
[∥]Innovation Center of NanoMedicine, Kawasaki Institute of Industrial Promotion, Kawasaki, Kanagawa 210-0821, Japan
[⊥]Department of Life Sciences, Program in Biological Sciences, European University Cyprus, Nicosia 1516, Cyprus
[#]Exploratory Oncology Research & Clinical Trial Center, National Cancer Center, Kashiwa, Chiba 277-8577, Japan
[¶]Department of Hepatobiliary-Pancreatic Surgery, National Cancer Center Hospital East, Kashiwa, Chiba 277-8577, Japan
[$]Department of Radiation Oncology, School of Medicine, University of Colorado, Aurora, Colorado 80045, United States
[△]Institute for Future Initiatives, The University of Tokyo, Bunkyo, Tokyo 113-0033, Japan

Supporting Information

ABSTRACT: **Dexamethasone is a glucocorticoid steroid with anti-inflammatory properties used to treat many diseases, including cancer, in which it helps manage various side effects of chemo-, radio-, and immunotherapies. Here, we investigate the tumor microenvironment (TME)-normalizing effects of dexamethasone in metastatic murine breast cancer (BC). Dexamethasone normalizes vessels and the extracellular matrix, thereby reducing interstitial fluid pressure, tissue stiffness, and solid stress. In turn, the penetration of 13 and 32 nm dextrans, which represent nanocarriers (NCs), is increased. A mechanistic model of fluid and macromolecule transport in tumors predicts that dexamethasone increases NC penetration by increasing interstitial hydraulic conductivity without significantly reducing the effective pore diameter of the vessel wall. Also, dexamethasone increases the tumor accumulation and efficacy of ∼30 nm polymeric micelles containing cisplatin (CDDP/m) against murine models of primary BC and spontaneous BC lung metastasis, which also feature a TME with abnormal mechanical properties. These results suggest that pretreatment with dexamethasone before NC administration could increase efficacy against primary tumors and metastases.**

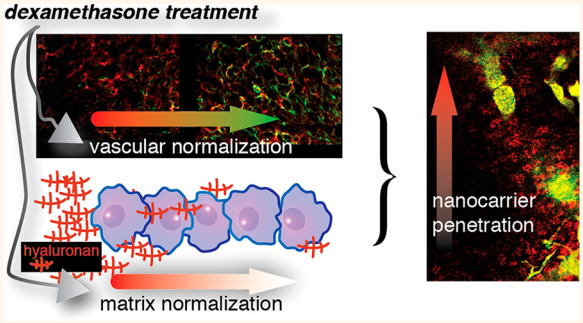

KEYWORDS: *tumor microenvironment, polymeric micelle, normalization, penetration, metastasis*

Nanocarriers (NCs) accumulate in tumors through the enhanced permeability and retention (EPR) effect[1] along with other complementary mechanisms, such as

Received: October 15, 2018
Accepted: June 6, 2019
Published: June 12, 2019

DOI: 10.1021/acsnano.8b07865
ACS Nano 2019, 13, 6396–6408

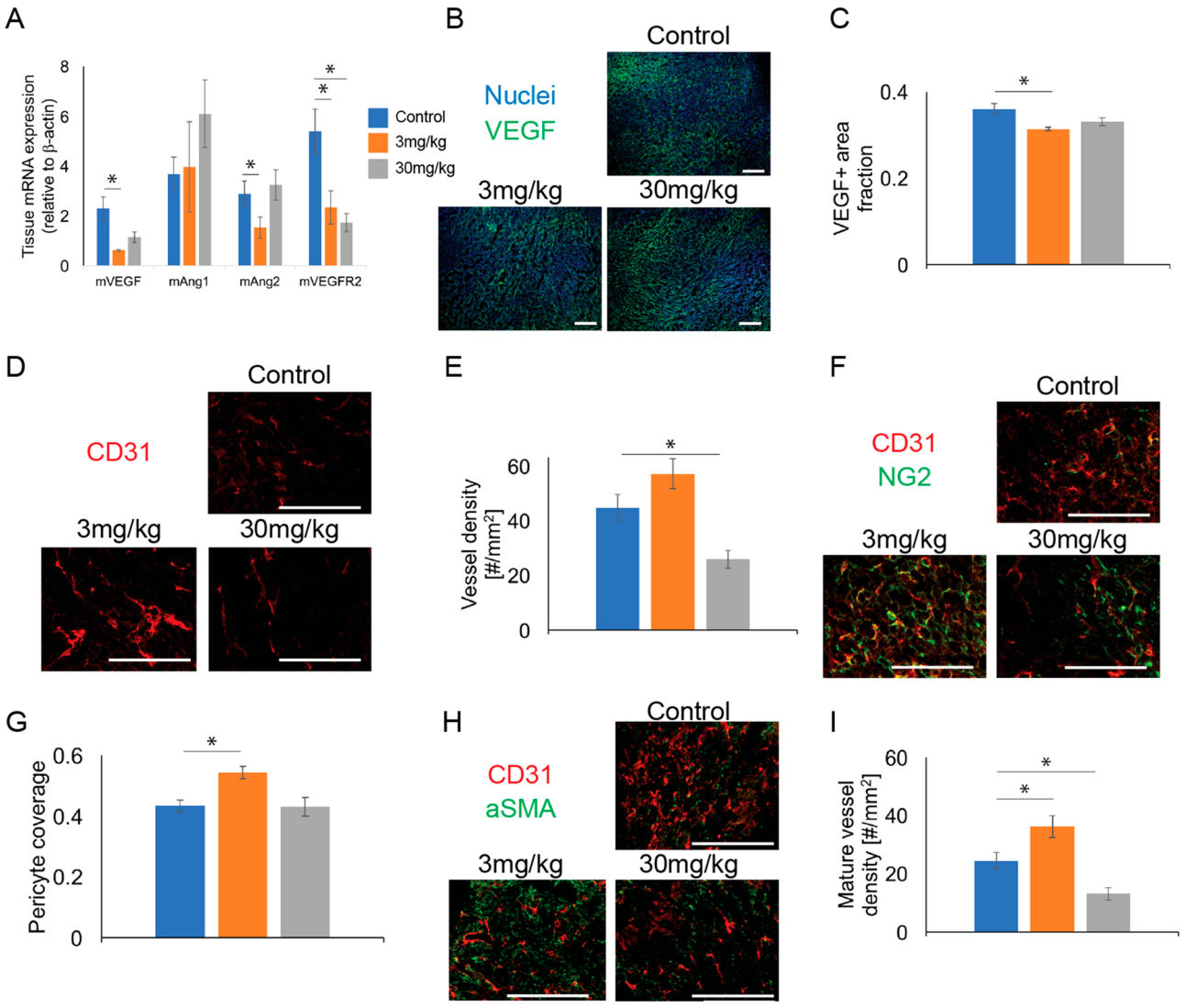

Figure 1. Dexamethasone induces vascular normalization. (A) Quantification of whole tumor mRNA expression of VEGF, Ang1, Ang2, and VEGFR2 in mice treated with 3 mg/kg (orange bars) and 30 mg/kg (gray bars) dexamethasone daily for 4 days compared to control mice (blue bars) as measured by RT-PCR (N = 8−9). (B) Representative images of VEGF (green) with nuclear counterstain (blue) immunofluorescence. (C) Quantification of area fraction positive for VEGF immunofluorescence staining (N = 4). (D) Representative images of CD31 (red) immunofluorescence marking tumor vessels. (E) Immunohistological quantification of the tumor vessel density, as assessed by the number of vessels normalized to the image area (N = 4). (F) Representative images of CD31 (red) and NG2 (green) immunofluorescence marking endothelial cells and pericytes, respectively. Yellow areas indicate colocalization of both cell types. (G) Quantification of the pericyte coverage of microvessels, as assessed by the fraction of CD31-positive staining area that is also positive for NG2 (N = 4). (H) Representative images of CD31 (red) and αSMA (green) immunofluorescence marking endothelial cells and pericytes/fibroblasts, respectively. Yellow areas indicate colocalization of both cell types. (I) Quantification of the density of mature vessels, as assessed by the density of vessels associated with αSMA+ cells (N = 4). All data expressed as mean ± standard error of the mean (*, P < 0.05). Scale bar = 100 μm.

vascular transcytosis.[2,3] In breast cancer (BC) patients, there is an association between NC accumulation and tumor shrinkage.[4] Nonetheless, there is heterogeneity of NC accumulation between various regions of a single tumor, different metastatic lesions in the same patient, and tumors of the same type in different patients.[2,4] Further, after NCs accumulate, preclinical evidence indicates that the intratumoral NC penetration from tumor blood vessels is limited and heterogeneous.[5,6] As NCs and other nanosized therapies are in clinical practice, translatable strategies that increase the magnitude of their accumulation and penetration while reducing heterogeneity of microdistribution may improve treatment outcomes.

One such strategy to increase and conform NC penetration and accumulation involves normalizing the noncancerous components of the tumor, which collectively are known as the tumor microenvironment (TME).[1,5] The function of tumor vessels, which deliver NCs to tumors, is compromised because they are leaky and compressed. Cancer cells stimulate unending pathological angiogenesis, leading to immature, leaky vessels. Cancer cells' subsequent unchecked proliferation generates mechanical forces that are stored and transmitted by the extracellular matrix (ECM), which is produced and maintained by contractile cancer-associated fibroblasts (CAFs).[7] These forces are applied within the tumor and to the surrounding tissue as solid stress, which is responsible for vessel compression.[5] Compression contributes to compromised vessel function, which in turn causes hypoxia, leading to treatment resistance.

DOI: 10.1021/acsnano.8b07865
ACS Nano 2019, 13, 6396−6408

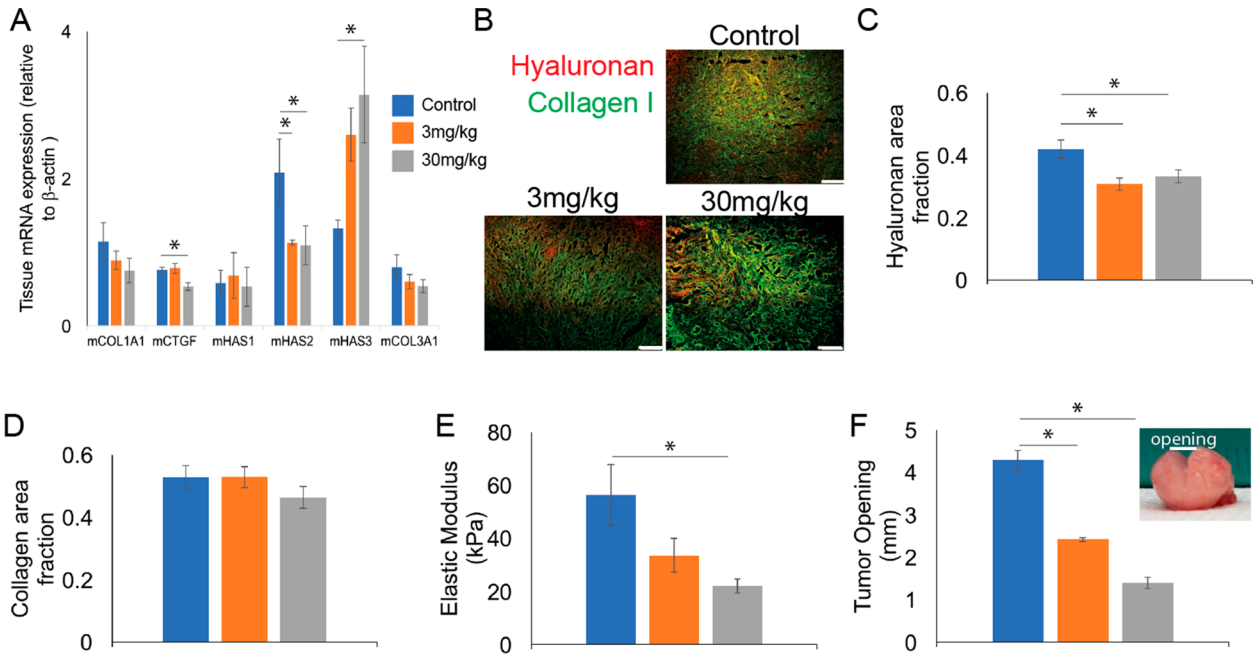

Figure 2. Dexamethasone induces ECM normalization. (A) Whole tumor mRNA expression of ECM-related cytokines as measured by RT-PCR in mice treated with 3 mg/kg (orange bars) and 30 mg/kg (gray bars) dexamethasone daily for 4 days compared to control mice (blue bars, N = 8−9). (B) Representative images of hyaluronan (red) and collagen I (green) immunofluorescence. Yellow areas indicate colocalization of both ECM components. (C) Quantification of area fraction positive for hyaluronan immunofluorescence (N = 4). (D) Quantification of area fraction positive for collagen I immunofluorescence (N = 4). (E) Quantification of tumor tissue elastic modulus, which is a measure of stiffness (N = 4). (F) Quantification of solid stress levels, which was assessed by length of the tumor opening after cutting the tissue (N = 4). All data expressed as mean ± standard error of the mean (*, P < 0.05). Scale bar = 100 μm.

Thus, normalizing vessels and CAFs/ECM represents an urgent need in the treatment of solid tumors.[8]

Preclinical studies demonstrate that normalizing vessel leakiness without pruning increases intratumoral transport of oxygen and NCs up to at least ~40 nm in diameter,[5,9,10] whereas normalization of CAFs and ECM toward vessel decompression increases delivery of NCs of all sizes, up to 125 nm.[5,11,12] Here, we identify a therapy that promotes both vessel and ECM normalization and is already commonly used in cancer patients, including those receiving cisplatin-loaded polymeric micelles (CDDP/m).[13] Specifically, we found that the glucocorticoid steroid dexamethasone, which is often given to patients post-chemo, immune or radiation therapy to manage toxicities, normalizes vessels and ECM. As a result, dexamethasone also normalizes the mechanical TME (*i.e.*, the material properties of the tumor tissue as well as the fluid and solid stressed applied to and by the tumor) as measured as reductions in interstitial fluid pressure (IFP), tissue stiffness, and solid stress. These effects increase the permeability of BC vessels to NCs, thereby improving treatment outcomes, even in murine models of spontaneous metastasis after primary tumor resection. We employed a fundamental mechanistic mathematical model to generate hypotheses to explain the complementary effects of vessel and ECM normalization on vessel permeability to NCs. We conclude that dexamethasone normalizes the mechanical TME toward increasing vessel permeability and potentiating NC-based chemotherapy. Our results indicate that dexamethasone treatment before chemotherapy administration can be re-evaluated to promote NC efficacy.

RESULTS AND DISCUSSION

Dexamethasone Blocks Angiogenesis Signaling and Normalizes Tumor Vessel Morphology. Vascular endothelial growth factor (VEGF) is the major driver of angiogenesis, which is a cause of the pathophysiology of tumor vessels, and blocking it promotes vascular normalization.[14] Dexamethasone reduces VEGF expression in murine models of brain cancer,[15] and we confirmed it would do so in 4T1 BC.[16] We treated immunocompetent BALB/c mice bearing orthotopic 4T1 BC daily for 4 days with 3 or 30 mg/kg dexamethasone.[17] This dose schedule was selected based on a previous work, which identified 3 mg/kg as the lowest dose that reduces IFP.[17] Additionally, we wanted to use a dose similar to that of the clinical trials of CDDP/m (NCT02043288),[13] which requires 20 mg of dexamethasone at 12 and 6 h before CDDP/m. By converting doses from human to mouse based on body surface area, each 20 mg dose in humans is equivalent to 4.11 mg/kg in mice. After CDDP/m, human patients receive 4 mg twice daily for 2 days, which is equivalent to 0.82 mg/kg in mice. Thus, the total dose of our regimen in mice and in the clinical trial are within 4% of each other (Supporting Information Table S1).

The mRNA expression of angiogenic signals in 4T1 tumors was determined by real-time polymerase chain reaction (RT-PCR). The results confirmed that the mRNA levels of VEGF were reduced along with other pro-angiogenic factors, such as angiopoietin 2 and VEGF receptor 2 (Figure 1A). Dexamethasone also reduced the protein levels of VEGF as assessed by immunofluorescence staining of tumor sections (Figure 1B,C). We next tested the effect of dexamethasone on vessel structure by using histology. Dexamethasone at 30 mg/kg reduced the microvessel density (Figure 1D,E), whereas dexamethasone at 3 mg/kg avoided pruning yet increased vessel maturity, as

DOI: 10.1021/acsnano.8b07865
ACS Nano 2019, 13, 6396−6408

indicated by the association of NG2+ pericytes with CD31+ endothelial cells (Figure 1F,G). As a result, 3 mg/kg dexamethasone increased the density of αSMA+ vessels (Figure 1H,I), which is a potential predictive biomarker of response to antiangiogenic therapy in human BC.[18] Thus, mRNA expression and histology experiments indicate that dexamethasone normalizes vessels.

Dexamethasone Normalizes the ECM and Mechanical TME. We then tested whether dexamethasone normalizes ECM. We focused on collagen I and hyaluronan because they have been identified as matrix components that contribute to solid stress and vessel compression.[7,11] Assessed by RT-PCR, dexamethasone reduced mRNA expression of hyaluronan synthase 2 levels but not those related to collagen (Figure 2A). Compensatory expression of hyaluronan synthase 3 was also observed, which corresponds with previous reports.[19] We also confirmed the protein expression of hyaluronan (Figure 2B,C) and collagen I (Figure 2B,D) in the tumors by histological staining. In this immunohistological analysis, only hyaluronan levels were reduced. Based on these results, we tested whether the mechanical TME was normalized. We found that 30 mg/kg dexamethasone reduced tissue stiffness, as measured by the elastic modulus, whereas 3 mg/kg only produced a trend (Figure 2E). On the other hand, by using the tumor-opening assay, which indicates the amount of residual stress held within the tumor tissue by the amount it opens after cutting,[7] we confirmed that both doses reduced solid stress (Figure 2F and Suppporting Information Figure S1). A larger opening is associated with more solid stress. Moreover, a single 3 mg/kg dose on the day of measurement did not reduce solid stress (Supporting Information Figure S2), which indicates that the pretreatment is necessary for ECM remodeling. Thus, the results from the mRNA expression, histology, and mechanical experiments suggest that dexamethasone normalizes the ECM in tumors by reducing hyaluronan levels.

Dexamethasone Normalizes Vessel Function. We then studied whether these structural and mechanical changes in the TME resulted in normalized vessel function. Previously, dexamethasone was shown to reduce IFP,[17] which is consistent with the data indicating that dexamethasone normalizes vessels (Figure 1) and ECM (Figure 2). We confirmed dexamethasone reduces IFP in 4T1 tumors (Figure 3A). Then, we performed intravital microscopy and assessed the morphology of perfused vessels after intravenous administration of a fluorescent dextran. Antiangiogenic therapies inducing vascular normalization reduce vessel diameters,[20] whereas ECM normalization reduces solid stress, leading to vessel decompression,[7] thereby increasing vessel diameters. We found that 3 mg/kg dexamethasone increased the average diameter of the perfused vessels (Figure 3B and Supporting Information Figure S3). We pooled by treatment group the perfused vessels imaged using intravital microscopy and assessed the distributions of diameters and lengths. Observation of the distribution of diameters of perfused vessels reveals the wide range of vessels produced by 3 mg/kg dexamethasone (Supporting Information Figures S3 and S4). Compared to the control, 30 mg/kg dexamethasone skews the distribution toward vessels with smaller diameters. Thus, the effects of 3 mg/kg dexamethasone on the distribution of vessel diameters indicates both vascular and ECM normalization. In contrast, the effects of 30 mg/kg indicate more vessel normalization relative to ECM normalization. Additionally, wide distribution of vessel length is suggestive of an orderly, branched vessel hierarchy present in normal tissue.[21] We found

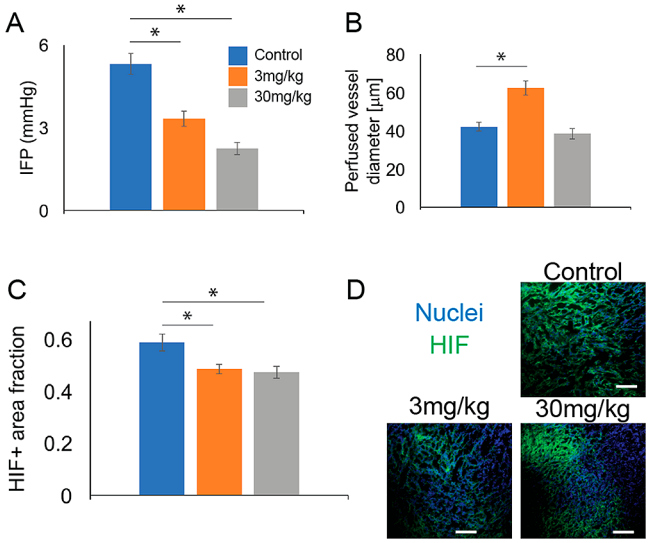

Figure 3. Dexamethasone normalizes vessel function. (A) IFP levels in mice treated with 3 mg/kg (orange bars) or 30 mg/kg (gray bars) dexamethasone daily for 4 days compared to control mice (blue bars, $N = 4$). (B) Average diameters of perfused tumor vessels as assessed by intravital microscopy ($N = 3$, $n = 175-220$ vessels per group). (C) Quantification of area fraction of HIF-1α immunofluorescence ($N = 4$). (D) Representative images of HIF-1α (green) with nuclear counterstain (blue) immunofluorescence. All data expressed as mean ± standard error of the mean (*, $P < 0.05$) Scale bar = 100 μm.

that 3 mg/kg dexamethasone-treated tumors had a wider, more even distribution of vessel lengths (Supporting Information Figures S3 and S5). Finally, we found dexamethasone reduced hypoxia signaling, as indicated by histological assessment of hypoxia-inducible factor 1α (HIF-1α) (Figure 3C,D). Thus, dexamethasone normalizes vessel function, leading to decreased hypoxia signaling.

Dexamethasone Improves NC Transvascular Transport. After confirming that dexamethasone normalizes vascular structure, ECM, and vessel function, we next hypothesized that dexamethasone would affect the rate NCs transport across tumor vessels and penetrate toward cancer cells. Transvascular transport depends on several factors: (i) the transvascular pressure gradient, which is a function of IFP; (ii) the hydraulic conductivity of the vasculature, which is a function of vessel maturity (*i.e.*, vessel wall pore diameter); and (iii) the hydraulic conductivity of the interstitial space, which is a function of ECM levels.[5,10,22−25] To investigate this, we performed continuous intravital microscopy on mice bearing orthotopic 4T1 tumors pre- and postinjection of fluorescent dextrans with 70 kDa (~13 nm hydrodynamic diameter, red) and 500 kDa molecular weight (~32 nm, green) (Figure 4A−D).[6] One hour postinjection, there was little penetration of the probes that accumulated outside the vessels in control tumors (Figure 4A); the pretreatment with 3 mg/kg dexamethasone induced deep penetration consistently in regions of perfused vessels (Figure 4B), and 30 mg/kg dexamethasone featured only few vessels enabling deep penetration (Figure 4C). From the intravital microscopy images, we quantified the penetration rate as the effective permeability.[10] Specifically, we segmented the extravascular (*i.e.*, interstitial) and intravascular space and measured the fluorescent signal in each region over time while quantifying the vascular surface area. From these data, we calculated the effective permeability as the rate of NC fluorescent signal passing through

DOI: 10.1021/acsnano.8b07865
ACS Nano 2019, 13, 6396−6408

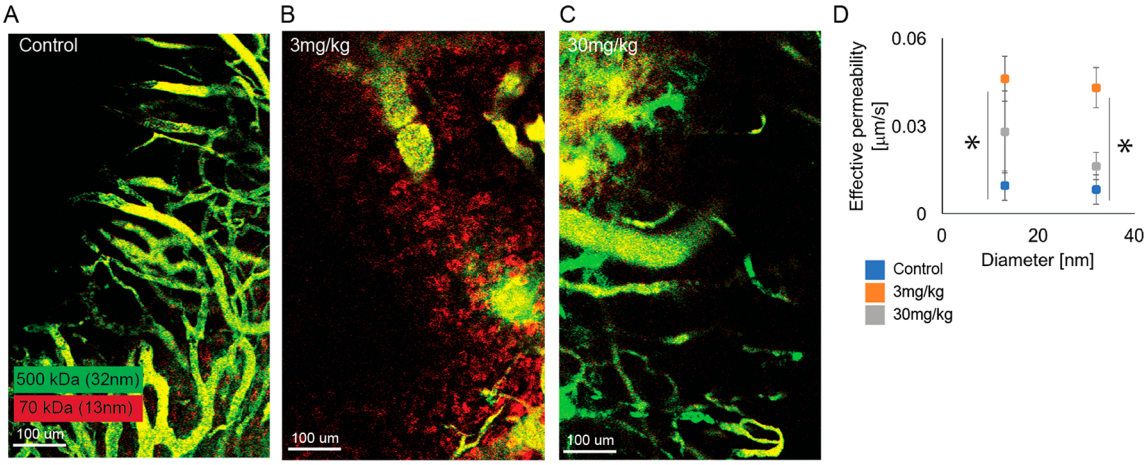

Figure 4. Dexamethasone increases the transvascular transport of nanocarriers. (A−C) Representative confocal intravital microscopy images of 4T1 tumors treated with four daily doses of (A) control, (B) 3 mg/kg, or (C) 30 mg/kg dexamethasone 1 h after co-injection of 70 kDa (13 nm, red) and 500 kDa (32 nm, green) fluorescent dextrans. (D) Quantification of effective permeability, which is a measure of the rate that dextrans are transporting out of vessels and penetrating after treatment with daily dexamethasone 3 mg/kg (orange), 30 mg/kg (gray), and control (blue, $N = 3-4$). Data expressed as mean ± standard error of the mean (*, $P < 0.05$).

the vessel walls normalized to the vessel surface area and the transvascular concentration difference (Supporting Information mathematical model). We found that only 3 mg/kg dexamethasone enhanced this rate compared to controls (Figure 4D). In a separate experiment, we found there was no increased penetration of 500 kDa dextrans with 0.3 mg/kg dexamethasone daily treatment (Supporting Information Figure S6A,B). Also, there was no increased penetration of doxil (∼80 nm) with 3 mg/kg dexamethasone daily treatment (Supporting Information Figure S7A,B). We also tested these findings in MDA-MB-231 breast tumors. As in 4T1 tumors, only 3 mg/kg dexamethasone increased penetration of 500 kDa dextrans (Supporting Information Figure S6C,D). In contrast to the results in 4T1, there was increased penetration of doxil (∼80 nm) with 3 mg/kg dexamethasone daily treatment (Supporting Information Figure S7C,D). Thus, these results suggest that whether dexamethasone increases NC transvascular transport depends on the dose of dexamethasone, the size of the NC, and the tumor. Additionally, they indicate that 3 mg/kg is an appropriate dose to increase the penetration of ∼32 nm NCs in 4T1 and MDA-MB-231 models of BC.

Mathematical Model of Dexamethasone's Effect on NC Transvascular Transport. The manner in which the vessel and ECM normalization interact to modulate NC transvascular transport is not clear. Vessel normalization increases vessel maturity and thereby reduces vessel leakiness by shrinking vessel wall pores. As a result, the hydraulic conductivity of the vessel wall reduces. In other words, fluid moves more slowly through the vessel wall (Figure 5A). This effect alone would increase NC transvascular transport because the intravascular fluid pressure would be higher relative to the IFP, and the increased pressure gradient would push NCs into the extravascular space. Nonetheless, if the pores shrink too much, NCs are too big to move freely out of the vessels because of steric hindrances (Figure 5B).[10] In contrast, ECM normalization reduces ECM levels, thereby increasing the hydraulic conductivity of the interstitial space (Figure 5C). This effect increases the rate of fluid flow in the extravascular region, which results in reduced IFP and thus increases transvascular transport of NCs of all sizes by increasing the transvascular pressure gradient.[11,12] Thus, the relative amounts of vascular and ECM normalization as well as NC size affect whether TME normalization enhances NC transvascular transport.

Because dexamethasone induces both vascular and ECM normalization, to generate hypotheses regarding how it affects NC transport, we employed a mathematical tumor model that describes fluid and macromolecule transport[22−25] and solved the corresponding parameter estimation problems (see the Supporting Information for detailed methods and results). In brief, using the experimentally measured effective permeability for each treatment (Figure 4D), we obtained the transient probe concentration profiles. Based on these profiles, we solved a deterministic optimization problem to find the hydraulic conductivities of both the vessel wall and the interstitial space that correspond to the best fit between the mathematical model and the experimental data (Figure 5). The solutions obtained using the concentration profiles derived from the effective permeability of 500 kDa dextran predicts that 3 mg/kg dexamethasone has more modest effects on the vascular hydraulic conductivity (and thus the effective vessel pore diameter) than 30 mg/kg dexamethasone (Figure 5D), and both doses similarly increase interstitial hydraulic conductivity (Figure 5E). Specifically, the model predicts that 3 mg/kg dexamethasone slightly reduces the vascular hydraulic conductivity such that the effective average pore size reduces from 204 nm in control tumors to 185 nm. In contrast, 30 mg/kg dexamethasone reduces it to 116 nm. The model also predicts that 3 mg/kg dexamethasone increases the interstitial hydraulic conductivity from 2.97×10^{-7} to 1.63×10^{-6} cm^2/mm Hg·s, whereas 30 mg/kg dexamethasone increases it to 1.68×10^{-6} cm^2/mm Hg·s. Although these results are unproven experimentally, our model predicts that dexamethasone at 3 mg/kg avoids remodeling the vessels such that they would physically hinder NCs because the effective pore size is only reduced by ∼10% (compared to ∼45% with 30 mg/kg dexamethasone) (Figure 5D), yet this dose still increases the transport of NCs by increasing the rate of solute transport in the tumor interstitial space (Figure 5E).

Dexamethasone Increases Efficacy of NCs in Metastatic BC. Because dexamethasone increases the penetration of 500 kDa dextrans (Figure 4), we hypothesized it would increase the antitumor effect of a similarly sized cytotoxic NC. Thus, to

DOI: 10.1021/acsnano.8b07865
ACS Nano 2019, 13, 6396−6408

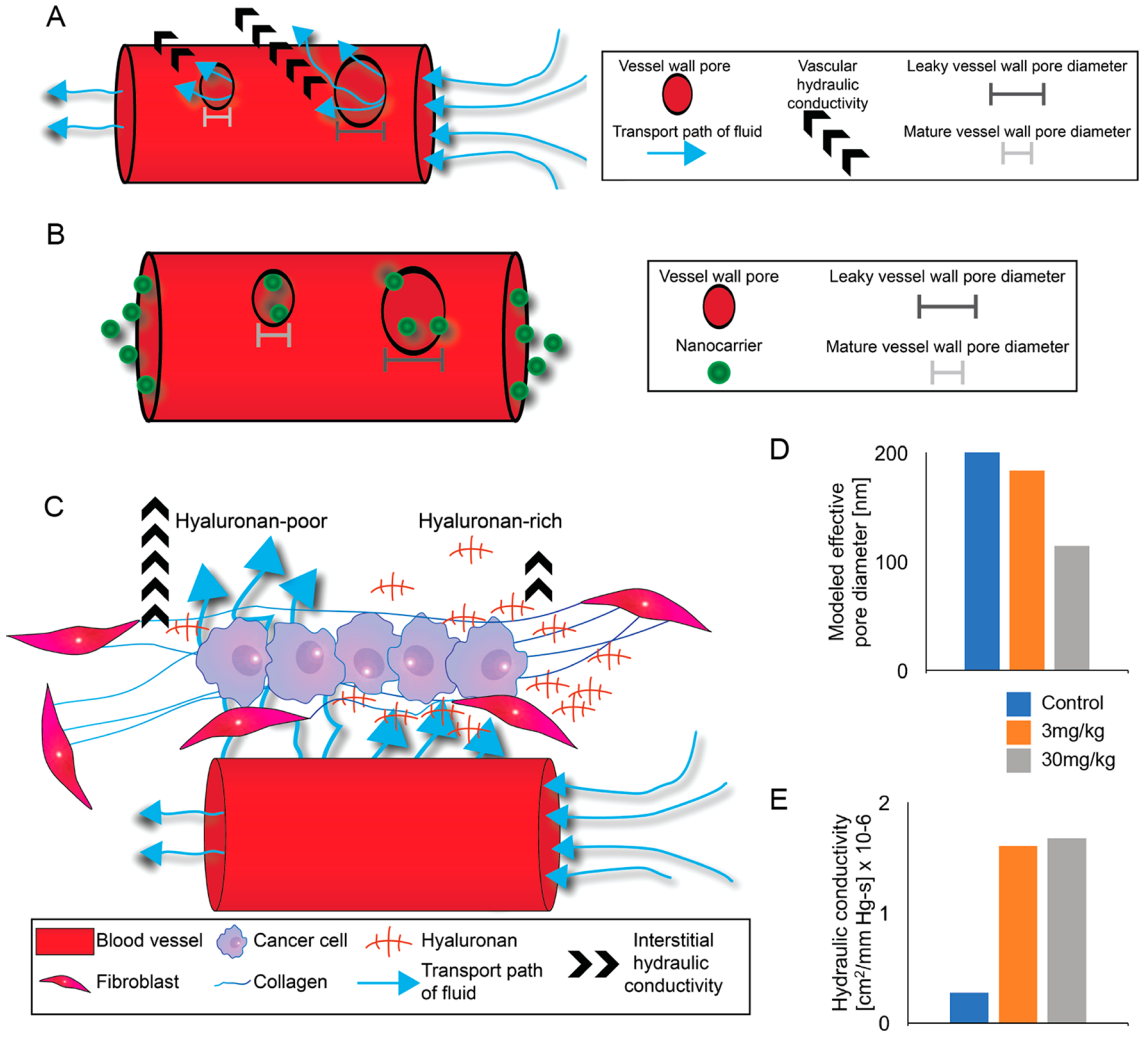

Figure 5. Model prediction of dexamethasone's effect on parameters related to transvascular transport. (A,B) Schematics of a vessel with a "leaky" vessel wall pore diameter (dark gray bar) and a "mature" vessel wall pore diameter (light gray bar), which are indicated by the relative size of the bar with the appropriate color. (A) Schematic of the dependence of vascular wall hydraulic conductivity on vessel wall pore diameter. Fluid flows (blue lines with single arrowhead) from right to left through the vessels and some enters the extravascular space through pores in the vessel wall. The vessel wall hydraulic conductivity (multiarrows) describes the ease that fluids percolate through the vessel wall. The length of the two multiarrows represents the relative magnitudes of hydraulic conductivity for each pore diameter. Fluid flow is impeded by the smaller vessel wall pore. (B) Nanocarriers (green spheres) flow through the vessel from right to left and extravasate through the pores. The leaky pore allows nanocarriers to pass through unimpeded, while the mature pore impedes extravasation physically. (C) Schematic of the dependence of interstitial hydraulic conductivity on hyaluronan levels. Fluid flows (blue lines with single arrowhead) from right to left through the vessels and some enters the extravascular space. The interstitial conductivity (magnitude indicated by multiarrows) is the ease that fluids percolate through the extravascular space, which is depicted as cells and matrix, given a specific pressure gradient (the driving force of convective flux). In the hyaluronan-rich region on the right, fluid percolation is reduced, whereas in the hyaluronan-poor region on the left, fluid percolation is increased. (D) Prediction of the effective vessel wall pore diameter of control (blue bar), 3 mg/kg (orange bar), and 30 mg/kg dexamethasone-treated (gray bar) tumors by the mathematical model. The model is solved using the data from the effective permeability experiments by varying the vascular and interstitial hydraulic conductivities. The vascular hydraulic conductivity is a function of vessel wall pore diameter. The predicted vascular pore diameter is based on the experimentally measured rate of probe transport, and thus, the pore diameter is not experimentally proven itself. (E) Prediction of interstitial hydraulic conductivity of control (blue bar), 3 mg/kg (orange bar), and 30 mg/kg dexamethasone-treated (gray bar) tumors by the mathematical model.

test our hypothesis, we used CDDP/m, which are ~30 nm. The addition of dexamethasone did not change the cytotoxicity of free cisplatin nor CDDP/m against 4T1 cells nor MDA-MB-231 cells (Table 1). Moreover, the combination of 3 mg/kg dexamethasone (as a daily 4 day dosing pretreatment) did not affect the circulation time of CDDP/m (Figure 6A) nor CDDP/m distribution to kidneys, liver, lungs, and spleen 24 h after injection (Supporting Information Figure S8).[26,27] Nonetheless, we found that, unlike a single dose of 3 mg/kg dexamethasone 2 h before CDDP/m administration, the 4 day pretreatment doubled the accumulation of CDDP/m in BC (Figure 6B). This is consistent with the finding that a single dose of dexamethasone 2 h before tumor excision did not reduce solid stress (Supporting Information Figure S2). We next tested the therapies in a primary tumor growth delay study against orthotopic 4T1-luc tumors, with an end point of days until 1000 mm^3 tumor volume. After correcting for multiple comparisons, we found that CDDP/m (1 mg/kg) monotherapy increased the number of days for the tumors to reach 1000 mm^3 compared to control (Figure 6C and Supporting Information Figure S9).

DOI: 10.1021/acsnano.8b07865
ACS Nano 2019, 13, 6396−6408

Table 1. *In Vitro* Cytotoxicity of Free Cisplatin (CDDP) and CDDP-Incorporated Micelle (CDDP/m) against 4T1 and MDA-MB-231 Cell Lines after 48 h Incubation

		IC_{50} (μM)[a,b]	
cell line	dexamethasone (μM)	CDDP	CDDP/m
4T1	1	5.3 ± 0.8	52 ± 3.7
	0.1	5.6 ± 0.5	60 ± 2.7
	0	4.4 ± 0.8	50 ± 6.0
MDA-MB-231	1	21.5 ± 3.1	168 ± 14.9
	0.1	21.8 ± 1.3	142 ± 8.3
	0	24.0 ± 1.0	139 ± 7.6

[a]Determined by a CCK8 kit. [b]Data presented as the mean ± SD (n = 4).

Combining dexamethasone with CDDP/m significantly increased this time period compared to that with CDDP/m monotherapy (Figure 6C and Supporting Information Figure S9). In mice bearing orthotopic MDA-MB-231 BC, the combination of dexamethasone and CDDP/m significantly extended the time to double the volume compared to CDDP/m alone (Figure 6D). Thus, dexamethasone enhances the efficacy of CDDP/m against 4T1-luc and MDA-MB-231 primary tumors. In addition, after the primary tumor growth delay experiment in 4T1-luc tumors, we assessed the metastatic burden in lungs and livers by luminescence imaging (Figure 6E–J). We found that the lungs (Figure 6I) and livers (Figure 6J) from the combination-treated mice had significantly less luminescence emission (total photon counts per second) than the organs from the control mice, demonstrating a profound antimetastatic effect.

From daily observation of body weight in the 4T1 study (Supporting Information Figure S10), we also found that the combination had led to a minor (less than 10% weight reduction) weight loss compared to the control group on the final day of the treatment regimen (Supporting Information Figure S11). Nonetheless, the body weight of mice returned to control levels by day 14 (Supporting Information Figure S11C). We also tested serum markers of kidney and liver toxicity (Supporting Information Figure S12) and found no evidence of toxicity induced by the combination. These results indicate the combination of dexamethasone with CDDP/m is safe and efficacious.

Dexamethasone Increases Efficacy of NCs in Pulmonary BC Metastases. Next, we investigated the effects of the combination of dexamethasone and CDDP/m on lung metastases. Specifically, we sought to assess whether the reduced metastatic burden with the combination treatment was a result of slower primary tumor growth or direct effects on metastatic lesions. In primary 4T1 BC tumors, our results indicate that dexamethasone increases the efficacy of CDDP/m in part by decompressing vessels. Compressed vessels are present in tumors of breast cancer patients,[11] and their abundance is a potential negative prognostic biomarker.[18,28] However, whether vessels are compressed in BC lung metastases is unclear. Thus, we first confirmed histologically in lung metastases from four BC patients that the vessels featured large aspect ratios (large diameter divided by short diameter), which is a measure of vessel compression (Figure 7A).[29] We next tested whether dexamethasone was active against lung metastases by measuring their mechanical properties. To mimic the clinical treatment protocol of metastatic disease and produce spontaneous metastases, we surgically removed 4T1 primary BC tumors when they reached ~300 mm^3. Then, after waiting 2 days postsurgery for the mice to rest and metastases to develop further, we administered dexamethasone daily for 4 days and then measured the stiffness of lungs. The lungs bearing metastases had high stiffness and reached almost half the value of primary BC tumors (Figure 7B), which indicates an abnormal mechanical TME. We found that dexamethasone reduced the stiffness of lungs (Figure 7B). Thus, we hypothesized that the combination of dexamethasone and CDDP/m might directly act against lung metastases. To prove this assumption, we followed the same protocol to produce murine models of metastasis after surgical removal of the primary tumor and administered two cycles of CDDP/m with daily dexamethasone. In these mice bearing 4T1 spontaneous metastases, we found that only the combination of dexamethasone and CDDP/m provided a survival advantage (Figure 7C). These experiments indicate that dexamethasone increases the efficacy of CDDP/m against BC pulmonary metastasis.

Discussion. Our results demonstrate the value of TME normalization in improving the efficacy of NCs. Although vessel-normalizing therapies are used clinically in combination with chemotherapy, they have limited effects on efficacy and can only improve delivery of small NCs. Furthermore, vascular normalization cannot alleviate hypoperfusion and reduced penetration caused by desmoplasia.[5] Specifically, vascular normalization cannot reverse vessel compression, which limits perfusion to large volumes of tissue within tumors.[8] By identifying dexamethasone as a therapy that normalizes both vessels and the ECM, we confirm that the combination of these strategies[8] is effective in potentiating the efficacy of cytotoxic NCs in models of metastatic BC. According to previous studies, these tumor models reflect both anti-VEGF-therapy-sensitive[30] (MDA-MB-231) and -resistant (4T1) cancers but might not represent the dense desmoplasia and lack of angiogenesis in pancreatic ductal adenocarcinoma.[31] Whether dexamethasone increases NC penetration likely will depend on its dose, the tumor type, and the size of the NC. Furthermore, our results highlight the need to supplement cytotoxic NCs with TME-normalizing therapies to treat pulmonary metastases, which are critical for patient survival yet have alternative mechanisms of resistance.[32]

Previous studies found that pretreatment dexamethasone increases the efficacy of certain chemotherapies.[33] These studies demonstrated that the effects of dexamethasone on the efficacy of small-molecule chemotherapies were the result of altered pharmacokinetics. Here, we did not observe a dexamethasone-induced change in pharmacokinetics of CDDP/m; however, NC formulations, such as CDDP/m, improve the pharmacokinetics of small-molecules. CDDP/m in particular is stable *in vivo* and has a long circulation time.[26] Here, we investigated the effects of dexamethasone on the mechanical TME and the changes in transport of NCs within tumors. Besides pharmacokinetics research, other studies reported negative effects of dexamethasone pretreatment on cytotoxicity. For example, in another breast cancer cell line, dexamethasone reduces the cytotoxicity of cisplatin.[34] In 4T1 and MDA-MB-231, we did not observe altered cytotoxicity of CDDP/m by dexamethasone.

In contrast to the pre-chemotherapy schedule we investigated, dexamethasone is often infused simultaneously with or within 1 day before chemotherapy to alleviate toxicities, including allergic reaction to platinum-based chemotherapies like CDDP/m.[13] Additional dexamethasone is administered post-chemotherapy if patients develop nausea. Nonetheless, various clinical evidence suggests that pre-chemotherapy dexamethasone could also help

DOI: 10.1021/acsnano.8b07865
ACS Nano 2019, 13, 6396–6408

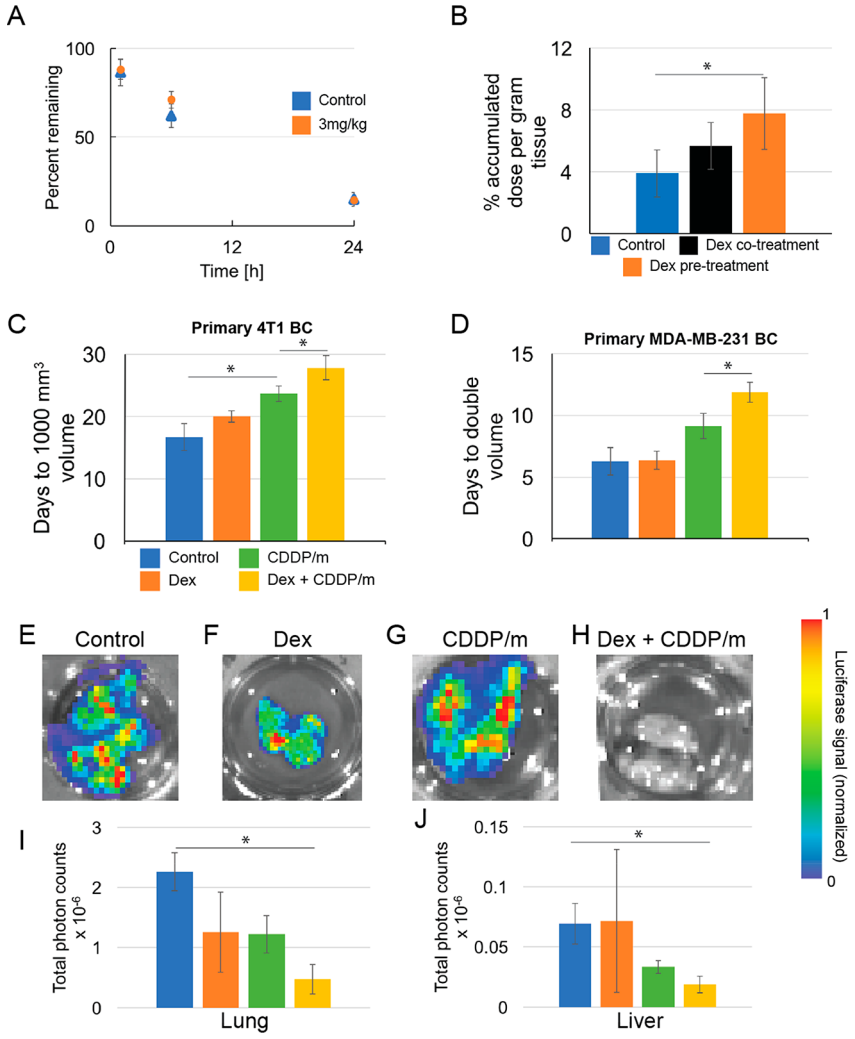

Figure 6. Dexamethasone increases the efficacy of 30 nm CDDP/m against metastatic breast cancer. (A) Time profile of percentage of platinum concentration remaining in the plasma collected at 1, 6, and 24 h after intravenous administration in control (blue triangles) and 3 mg/kg dexamethasone-treated (orange circles) mice ($N = 3$). (B) Tumor accumulation of platinum 24 h after administration of CDDP/m. Control-treated mice were compared to mice treated with 3 mg/kg dexamethasone daily for 4 days (orange bar) or once 2 h before CDDP/m administration (black bar, $N = 6$). (C) Quantification of tumor growth rate. Graph of the number of days between treatment initiation and 1000 mm^3 tumor volume in mice bearing 4T1-luc tumors. When tumors reached ∼90 mm^3, they were size- and time-matched into control (blue bar, equal volume of phosphate-buffered saline (PBS) and schedule to other treatments), dexamethasone monotherapy (orange bar, 3 mg/kg dexamethasone i.p. daily days 0−8), CDDP/m monotherapy (green bar, 1 mg/kg i.v. days 2, 5, and 8), and dexamethasone and CDDP/m combination (yellow bar) groups ($N = 6$). (D) Quantification of tumor growth rate. Graph of the number of days between treatment initiation and tumor volume doubling in mice bearing MDA-MB-231 tumors. When tumors reached ∼90 mm^3, they were size- and time-matched into control (blue bar, equal volume of PBS and schedule to other treatments), dexamethasone monotherapy (orange bar, 3 mg/kg dexamethasone i.p. daily days 0−8), CDDP/m monotherapy (green bar, 1 mg/kg i.v. days 2, 5, and 8), and dexamethasone and CDDP/m combination (yellow bar) groups ($N = 7$−8). (E−H) Representative images of *ex vivo* luminescence in lungs bearing 4T1-luc metastases from mice reaching the end point in the tumor growth delay study. (I,J) *Ex vivo* quantification of total luminescence photon counts. Only organs from mice with similar tumor volumes and days after treatment initiation were compared ($N = 3$). (I) Quantification of total luminescence photon counts in lungs. (J) Quantification of total luminescence photo counts in livers. All data expressed as mean ± standard error of the mean (*, $P < 0.05$).

prevent chemotherapy-induced toxicities. For example, dexamethasone pretreatment decreases hematopoietic toxicity and improves the efficacy of a chemotherapeutic regimen in patients with metastatic non-small cell lung cancer.[35−37] Also, dexamethasone reduces edema in brain cancer patients.[38] The current study suggests that commonly used chemotherapy adjunct treatments, such as dexamethasone, might affect NC therapy efficacy and highlights the potential of rescheduling dexamethasone before chemotherapy to increase NCs' efficacy, particularly in treatment-resistant pulmonary BC metastases. Dexamethasone's low cost and broad use in oncology highlight its potential impact as an adjunct to potentiate cancer nanomedicine.

CONCLUSIONS

Our results demonstrate that dexamethasone pretreatment can increase the tumor penetration of NCs with hydrodynamic diameters between ∼13 and ∼32 nm by normalizing the TME. This is achieved by the effects of dexamethasone on the tumor vessels and ECM, which results in a mechanical TME more amenable to NC transvascular transport. Our mathematical model based on the tumor penetration data suggests that the

DOI: 10.1021/acsnano.8b07865
ACS Nano 2019, 13, 6396−6408

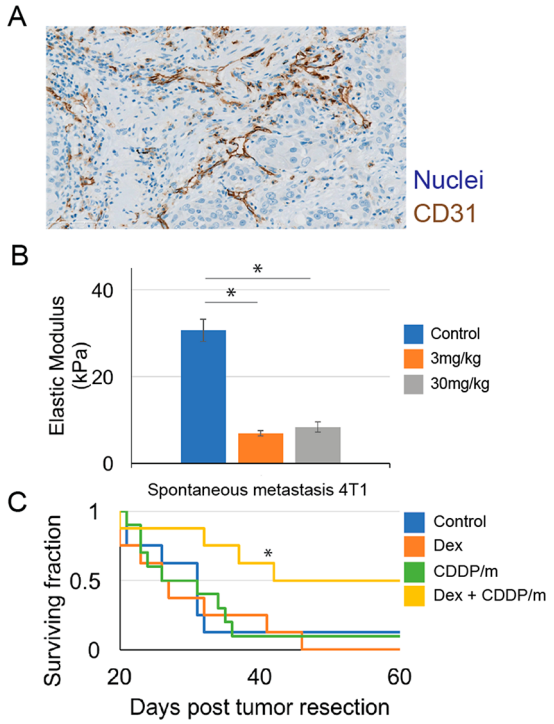

Figure 7. Dexamethasone increases the efficacy of 30 nm CDDP/m against lung metastases from breast cancer. (A) Representative image of histology of CD31 (brown) from the lung metastasis of a breast cancer patient. (B) Quantification of the 4T1 lung metastasis tissue elastic modulus, which is a measure of stiffness. Control-treated mice (blue bar) were compared to mice treated with 3 mg/kg (orange bar) and 30 mg/kg (gray bar) dexamethasone daily for 4 days. Data expressed as mean ± standard error of the mean (N = 5−7). (C) Animal survival in mice with spontaneous metastases from 4T1 primary tumors, which developed after surgical primary tumor resection at 300 mm^3. Mice were size- and time-matched into control (blue bar, equal volume and schedule of PBS as other treatments), dexamethasone monotherapy (orange bar, 3 mg/kg dexamethasone i.p. daily days 2−7 postresection), CDDP/m monotherapy (green bar, 1 mg/kg i.v. days 4 and 7 postresection), and dexamethasone and CDDP/m combination (yellow bar) groups (N = 8−10, *, P < 0.05).

increased NC transport from an appropriate dose of dexamethasone results from a modest reduction in effective pore diameter of the vessel wall and a more dramatic increase in interstitial hydraulic conductivity. Eventually, dexamethasone increased the delivery and antitumor activity of CDDP/m, a clinically used ∼30 nm NC, in primary BC tumors and their lung metastases. Thus, besides limiting some toxicities of anticancer drugs, dexamethasone can increase the efficacy of anticancer drug-delivering NCs.

METHODS

Cell Culture. For mechanical, histological, and gene expression studies, 4T1 mouse mammary carcinoma cell line was purchased from ATCC. For intravital microscopy, biodistribution, and efficacy studies, 4T1 cells expressing luciferase (4T1-luc) were purchased from Japanese Collection of Research Bioresources Cell Bank (Osaka, Japan). The cells were maintained at 37 °C/5% CO_2 and cultured in Dulbecco's modified Eagle's medium (DMEM) supplemented with 10% fetal bovine serum and 1% streptomycin/penicillin.

Drugs and Reagents. Dexamethasone sodium phosphate (Sigma-Aldrich, St. Louis, USA) was solubilized with sterile water at 37 °C.[17] Doxil was purchased from Alza Corporation (Vacaville, CA). α-Methoxy-ω-aminopropyl-poly(ethylene glycol) (MeO-PEG-NH_2; M_w = 12 000) was purchased from NOF Co., Inc. (Tokyo, Japan). γ-Benzyl-L-glutamate *N*-carboxyanhydride (BLG-NCA) was purchased from Chuo Kaseihin Co., Inc. (Tokyo, Japan). Acetic anhydride (>97%), sodium hydroxide (96%), and *N*,*N*-dimethylformamide (DMF) were purchased from Wako Pure Chemical Industries Ltd., (Osaka, Japan). *cis*-Diamminedichloroplatinum(II) (CDDP) was purchased from Aldrich Chemical Co., Inc. Poly(ethylene glycol)-*block*-poly(L-glutamic acid) (PEG-*b*-P(Glu); $M_{n,PEG}$ = 12 000 g/mol, DP P(Glu) = 40, M_w/M_n = 1. 10) and cisplatin micelles (CDDP/m) were prepared as described previously.[27] A mixture of PEG-*b*-P(Glu) and CDDP ([Glu] = [CDDP] = 5 mM) was stirred at 37 °C for 5 days. Any unloaded free CDDP was removed by dialysis (molecular weight cutoff size = 8000 Da) with distilled water and further purified by ultrafiltration [molecular weight cutoff size (MWCO) = 100 000) and passed through a 0.22 μm PES filter. Diameter and polydispersity index (PDI) of micelles were measured using a dynamic laser scattering spectrometer at 25 °C using a Zetasizer Nano-ZS instrument (Malvern Instruments, Malvern, UK) equipped with a He−Ne ion laser (at wavelength 532 nm) with detection angle equal to 90° at 37 °C. The average diameter was 30 nm with a PDI of 0.18.

Animal Tumor Models. Female 6 week old BALB/c (for 4T1 studies) and BALB/c nu/nu mice (for MDA-MB-231 studies) were purchased from Charles River Co. (Tokyo, Japan). All the experiments were conducted under the ethical guidelines of The University of Tokyo, of the Innovation Center of NanoMedicine (Kawasaki, Japan), and of the Republic of Cyprus and the European Union under a license acquired by the Cyprus Veterinary Services (No. CY/EXP/PR.L1/2014), the Cyprus national authority for monitoring animal research. Orthotopic models for murine mammary tumors were generated by implantation of 5 × 10^4 4T1 or 4T1-luc and 1 × 10^7 MDA-MB-231 mouse mammary cancer cells in 40 μL of serum-free medium into the third mammary fat pad of 6 week old BALB/c and BALB/c nu/nu female mice, respectively. Once tumors grew past 6 mm in diameter, tumors were extracted and 1 mm^3 chunks of tumors were implanted for all *in vivo* studies. Serial solid passages were limited to three times.

Fluorescent Immunohistochemistry. For histological studies, dexamethasone (3 mg/kg or 30 mg/kg) or equal volume PBS was administered by intraperitoneal (i.p.) injection once a day for 4 days starting from day 7 to day 11 postimplantation and before tumor excision. 4T1 breast tumors were removed, incubated with 4% paraformaldehyde for 40 min, and washed twice for 10 min with 1× PBS. Fixed tissues were embedded in optimal cutting temperature compound in cryomolds (Tissue-Tek) and frozen completely at −20 °C. Transverse 20 μm thick tumor sections were produced using the Tissue-Tek Cryo3 (SAKURA). Positively charged HistoBond microscope slides (Marienfeld) were used to bond four tissue sections per tumor. Tumor sections were then incubated in blocking solution (10% fetal bovine serum, 3% donkey serum, 1× PBS) for 2 h and immunostained with the following primary antibodies; rabbit anticollagen I (ab4710, Abcam 1:100), sheep antihyaluronic acid (ab53842, Abcam 1:100), rat anti-CD31 (MEC13.3, BD Pharmingen 1:100), and rabbit-αSMA (ab5694, Abcam 1:100), mouse anti-VEGF (C-1) (sc-7269, Santa Cruz 1:50), anti-mouse HIF-1α (H1alpha67, 1:100), and rabbit anti-NG2 (AB5320, Millipore 1:200) overnight at 4 °C. For murine antibodies, tumor sections were blocked with unconjugated Fab fragment anti-mouse IgG (H+L) (Jackson ImmunoResearch) to suppress the off-target signal from any endogenous mouse Ig prior to the overnight incubation with the mouse primary antibodies. Secondary antibodies against rabbit, sheep, or rat conjugated to Alexa Fluor 488 and 647 (Invitrogen) were used at 1:400 dilution, except the secondary antibody against mouse conjugated to Alexa Fluor 488 (A21202, Invitrogen) was used at 1:300 dilution. All samples were incubated in secondary antibody solution including DAPI (Sigma, 1:100 of 1 mg/mL stock) for 2 h at room temperature in the dark. Sections were mounted on microscope slides using the ProLong gold antifade mountant (Invitrogen) and covered with a glass coverslip.

Histological Image Acquisition and Analysis. Images of stained tumor sections from the tumor interior and periphery were acquired at

DOI: 10.1021/acsnano.8b07865
ACS Nano 2019, 13, 6396−6408

10× magnification using an Olympus BX53 fluorescence microscope. To enable quantification, images of the same staining were taken at identical settings. The images were analyzed using custom and built-in algorithms in MATLAB (MathWorks, Inc., Natick, MA, USA). Specifically, VEGF, HIF-1α, collagen I and hyaluronan tumor composition was analyzed following calculation of the area fraction of positive staining using an in-house code in MATLAB. Similarly, the blood vessel density was measured by segmenting the CD31+ area using an intensity and size threshold. The CD31+ area was skeletonized to count vessels and normalized to the total tissue area within the image. Pericyte coverage with NG2 was assessed as the fraction of NG2+ area within the total CD31+ area. Mature vessel density was measured similarly to the vessel density, except only vessels with greater than 10% αSMA+ area fraction were counted.

RNA Isolation, cDNA Synthesis, and Real-Time PCR. Total RNA was isolated from breast tumors according to the standard Trizol-based protocol (Invitrogen), and cDNA synthesis was performed using reverse transcriptase III (RT-III) enzyme and random hexamers (Invitrogen). Real-time polymerase chain reaction was performed using Sybr Fast Universal Master Mix (KAPA). The specific mouse primers used for gene expression analysis of 4T1 tumors are listed in the table below. Reactions were performed using a CFX-96 real-time PCR detection system (Biorad) at the following conditions: 95 °C for 2 min, 95 °C for 2 s, 60 °C for 20 s, 60 °C for 1 s, steps 2−4 for 39 cycles. Real-time PCR analysis and calculation of changes in gene expression between compared groups was performed using the $\Delta\Delta Ct$ method. Relative gene expression was normalized based on the expression of β-actin.

Table 2

gene name	primer sequence
mVEGF F	AGCACAGCAGATGTGAATGC
mVEGF R	TTTCTTGCGCTTTCGTTTTT
mAng1 F	CAGCACGAAGGATGCTGATA
mAng1 R	TTAGATTGGAAGGGCCACAG
mAng2 F	TCCAAGAGCTCGGTTGCTAT
mAng2 R	AGTTGGGGAAGGTCAGTGTG
mVEGFR2 F	CCCAGCATCTGGAAATCCTA
mVEGFR2 R	CCGGTTCCCATCTCTCAGTA
mCOL1A1 F	GAGCGGAGAGTACTGGATCG
mCOL1A1 R	GTTCGGGCTGATGTACCAGT
mCTGF F	CACTCTGCCAGTGGAGTTCA
mCTGF R	GTAATGGCAGGCACAGGTCT
mHAS1 F	TCGGAGATTCGGTGGACTAC
mHAS1 R	GTCCAACCTTGTGTCCGAGT
mHAS2 F	ATAAGCGGTCCTCTGGGAAT
mHAS2 R	CCTGTTGGTAAGGTGCCTGT
mHAS3 F	TTCCAAACCTCAAGGTGGTC
mHAS3 R	TGCTACGCCACACAAAGAAG
mCOL3A1 F	ATAAGCCCTGATGGTTCTCG
mCOL3A1 R	GCAGCCTTGGTTAGGATCAA
mβ-ACTIN F	GACGGCCAGGTCATCACTAT
mβ-ACTIN R	AAGGAAGGCTGGAAAAGAGC

Interstitial Fluid Pressure Measurement. Interstitial fluid pressure was measured *in vivo* with the wick-in-needle technique after administering anesthesia and before tumor excision, as described previously.[12]

Tumor-Opening Measurement. After initiating tumors with chunk implantations, dexamethasone (3 mg/kg or 30 mg/kg) or equal volume PBS was administered i.p. once a day for 4 days starting from day 7 to day 11 postimplantation and before tumor excision, so that the average tumor diameter for each tumor was between 0.6 and 1.1 cm. For dexamethasone co-administration, PBS was administered daily for 3 days, and 3 mg/kg dexamethasone was administered on the fourth day 2 h before tumor extraction. For the tumor-opening measurement, tumors were extracted and a cut was made along the tumor's longest axis (~80% of its thickness). This length was marked on the scalpel with tape to ensure a consistent cut. The tumor was then allowed to relax for 10 min to allow for any transient, poroelastic response to diminish and the opening at the surface of the tumor was measured.[7]

Mechanical Testing Measurements for Calculation of Elastic Modulus. For primary tumor studies, dexamethasone (3 or 30 mg/kg) was administered by i.p. injection once a day for 4 days starting from day 7 to day 11 postimplantation and before tumor excision. For the study of the mechanical properties of lung metastases, after removal of primary tumors on day 27 (tumor volume of ~300 mm^3), dexamethasone was administered by i.p. injection once a day for 4 days starting from day 29 to day 32 postimplantation (the day of lung excision). Measurement of the elastic modulus was performed using an unconfined compression experimental protocol.[12,19] Following excision of the primary tumor or the macroscopic metastatic nodules, specimens were loaded on a high precision mechanical testing system (Instron, 5944, Norwood, MA, USA) and compressed to a final strain of 30% with a strain rate of 0.1 mm/min. The dimensions of the primary tumor specimens were 6 × 6 × 4 mm (length × width × thickness), whereas metastatic nodules were tested in whole owing to their small size. The elastic modulus was calculated from the slope of the stress−strain curve at the 25−30% strain range.[12,19]

***In Vivo* Confocal Laser Scanning Microscopy.** Chunks of 4T1 or MDA-MB-231 tumors (1 mm^3) were implanted into the third mammary fat pad, and treatment was initiated when the tumors reached ~90 mm^3. Tumors were matched for time postimplantation and size at treatment initiation. Dexamethasone at 0.3, 3, or 30 mg/kg or equal volume PBS was administered daily for 4 days. After surgical exposure of the orthotopic 4T1 or MDA-MB-231 tumor using the skin flap method, mice were intravenously co-injected with 70 kDa rhodamine-bound (Sigma-Aldrich, St. Louis, USA) and 500 kDa FITC-bound dextran (Sigma-Aldrich, St. Louis, USA) at volumes of 0.1 mL each and doses of 0.16 and 0.04 mg, respectively. Doxil was administered at 7 mg/kg. Microscope settings and probe concentrations were adjusted to make the fluorescence signal equal and remained unchanged for each probe. All *in vivo* image acquisitions were performed using a Nikon A1R confocal laser scanning microscope system attached to an upright ECLIPSE FN1 (Nikon).

Image Analysis. Images were analyzed using custom analysis software developed in MATLAB (The MathWorks). The normalized transvascular flux[9] was calculated using

$$\frac{J_t}{\frac{S}{V}(C_v - \hat{C})} = P_{eff} = \lim_{\hat{t}\to 0} \frac{\partial}{\partial \hat{t}} \frac{\int_{\hat{r}=\hat{R}}^{\infty} \hat{C}(\hat{r})\hat{r}\partial\hat{r}}{(C_v - \hat{C})\hat{R}}$$

where J_t is the transvascular flux, $\hat{C}$ is the concentration of the probe immediately extravascular, P_{eff} is the effective permeability,[17] $\hat{t}$ is the time after the initial image, $\hat{r}$ is the distance from the vessel central axis, and $\hat{R}$ is the vessel radius at that point along the vessel. Fluorescence intensities were used as the concentrations. The calculation was made as an average over the entire imaged volume for each tumor. For the 2D case,[18] this equation simplifies to

$$P_{eff} = (1 - HT)\frac{V}{S}\left(\frac{1}{I_0 - I_b}\frac{dI}{dt} + \frac{1}{\kappa}\right)$$

where HT is the tissue hematocrit estimated to be 0.19 in the circulation of tumors, I is the average fluorescence intensity of the whole image, I_0 is the value of I immediately after the filling of all vessels, I_b is the background fluorescence intensity, and κ is the time constant of plasma clearance of the probe. The slope of the measurements plotted over time should be normalized, where dI/dt becomes $(dI/dt)/(I_0 - I_b)$. V and S are the total volume and surface area of vessels within the tissue volume covered by the surface image, respectively. The volume-to-surface ratio is calculated as

DOI: 10.1021/acsnano.8b07865
ACS Nano 2019, 13, 6396−6408

$$\frac{V}{S} = \frac{\sum_{n=1}^{M} L_n d_n^2}{\sum_{n=1}^{M} 4 d_n L_n^2}$$

where d_n is the diameter of the nth vessel and L_n is the length of the nth vessel corrected by a factor of 0.79 for light scattering in the tissue.

***In Vitro* Cytotoxicity.** The *in vitro* cytotoxicity of CDDP and CDDP/m with and without dexamethasone was examined against 4T1 and MDA-MB-231. Cancer cells were plated into flat-bottomed, 96-well plates at 2.5×10^3 cells per well. They were treated by continuous exposure to various concentrations of CDDP and CDDP/m in a final volume of 100 μL. Plates were incubated for 48 h at 37 °C in a humidified atmosphere with 5% CO2, and cell viability was determined by MTT assay.

Biodistribution Studies. After implantation of 4T1 tumor chucks into the third mammary fat pad, the treatment was initiated when tumors reached ~90 mm^3. Tumors were size- and time-matched for initiation into the study. Dexamethasone (3 mg/kg) or equal volume PBS was administered daily for 3 days by i.p. injection. On the fourth day, the same treatments were given except for the co-administration group, which was given dexamethasone. Two hours later, all mice were administered CDDP/m (5.5 mg/kg) by retro-orbital injection under inhaled isoflurane anesthesia. Twenty-four hours postinjection of CDDP/m, mice were sacrificed and exsanguinated. Tumors and normal organs were collected, weighed, and digested using boiling 90% HNO_3 followed by proper dilution with 1% HNO_3. The concentration of platinum was measured by inductively couple plasma mass spectrometry (ICP-MS) [Hewlett-Packard HP 4500 ICP-MS (Agilent Technologies, California, USA); RF power = 1200 W; peripump = 0.16 rps; monitoring mass = m/z 195 (Pt); integrating interval = 0.1 s; sampling period = 0.3 s]. Data were normalized against the total injected dose per tissue mass.

Efficacy Studies. For primary growth studies, 1 mm^3 chunks of 4T1-luc or MDA-MB-231 tumors were implanted in the third mammary fat pad of BALB/c or BALB/c nu/nu female mice, respectively, and treatment was initiated when tumors reached ~90 mm^3. Tumors were size- and time-matched for initiation into the study. Dexamethasone at 3 mg/kg was administered daily from days 0 to 8. CDDP/m at 1 mg/kg was administered by retro-orbital injection during sedation with isoflurane on days 2, 5, and 8. The tumors were measured every 1−2 days using calipers by an investigator blind of the treatment groups. For metastasis survival studies, 1 mm^3 chunks of 4T1-luc tumors were implanted and primary tumors were excised when tumors reached ~300 mm^3, which was defined as day 0. Excision was timed such that mice were initiated into the study by size- and time-matching their primary tumors. Two days after tumor removal, which allowed the mice to rest, treatment was initiated. Dexamethasone at 3 mg/kg was administered daily from days 2 through 7. CDDP/m at 1 mg/kg was administered by retro-orbital injection during sedation with isoflurane on days 4 and 7. Mice were monitored daily for the first 3 weeks of efficacy studies and every other day thereafter.

Luminescent Imaging Studies. After mice bearing 4T1-luc tumors reached the end point (primary tumor volume of 1000 mm^3), surviving mice were grouped to match time since treatment initiation and tumor volume. Based on these criteria, three mice from each group were included to produce an average tumor volume of ~1300 mm^3 and 28 days post-treatment initiation in each group. Mice were sacrificed 1 min after retro-orbital injection of luciferin salt solution. Lungs and livers were removed and imaged *ex vivo* using an IVIS Spectrum (SP-BFM-T1, PerkinElmer).

Serum Biomarkers. Mice were given dexamethasone and CDDP/m according to the primary tumor efficacy protocol. The blood samples of all mice were collected once every mouse in the study reached the end point of the efficacy study. The blood was centrifuged to take the serum. From each blood sample, plasma concentrations of alkaline phosphatase, alanine aminotransferase, aspartate aminotransferase, and blood urea nitrogen were measured by using a FUJI DRI-CHEM NX500 analyzer (FujiFilm, Japan).

Immunohistochemistry of Human Lung Metastases from Breast Cancer. Five metastatic tumors in lungs from four breast cancer patients were surgically resected. Four micrometer slides were obtained from surgically resected FFPE sample of metastatic tumor. Tissues were stained with monoclonal anti-human CD31 antibodies (Dako, Glostrup, Denmark). Immunostaining was performed using an autostaining machine (Ventana Benchmark ULTRA, Ventana Medical Systems, Tucson, AZ, USA), as reported previously. Stained slides were imaged using a NanoZoomer digital pathology virtual slide system. Three X30 JPEG photos from peritumoral and center areas of metastases were obtained as reported previously.[39] Morphological analysis was performed using morphometric software (WinROOF version 6.5, Mitani Corporation, Tokyo, Japan). CD31 endothelial cell clusters with and without lumen were counted.

Statistical Analysis. The data are presented as means with error bars representing the standard error of the mean. Groups were compared using unpaired Student's t tests, except in the metastasis survival study where a log-rank test was used. In studies with multiple pairwise comparisons, P values were adjusted using Holm-Bonferroni correction. Except in the efficacy studies, each treatment group was compared only with the control group.

ASSOCIATED CONTENT

Supporting Information

The Supporting Information is available free of charge on the ACS Publications website at DOI: 10.1021/acsnano.8b07865.

Description of the mathematical model, its results, and additional experimental results are described; Figures S1−S12 and Tables S1 and M1−M3 (PDF)

AUTHOR INFORMATION

Corresponding Authors

*E-mail: kataoka@ifi.t.u-tokyo.ac.jp.
*E-mail: horacio@bmw.t.u-tokyo.ac.jp.

ORCID

John D. Martin: 0000-0002-9828-8203
Matthew David Stuber: 0000-0001-8435-9552
Kazunori Kataoka: 0000-0002-8591-413X
Horacio Cabral: 0000-0002-4030-2631

Notes

The authors declare no competing financial interest.

ACKNOWLEDGMENTS

We thank Dr. Y. Mochida for critical comments on the manuscript, and Dr. X. Liu and Dr. T. Tockary for helpful discussions. This work was supported by fellowships from the Japan Society for the Promotion of Science (Nos. P16731 and PE14787 to J.D.M), the European Research Council Grant 336839 and INFRASTRUCTURE/1216/0052 co-financed by the European Regional Development Fund and the Republic of Cyprus through the Research Promotion Foundation (to T.S.), the Center of Innovation (COI) Program from Japan Science and Technology Agency (JST), the Practical Research for Innovative Cancer Control from Japan Agency for Medical Research and Development, AMED (to K.K.), as well as Grants-in-Aid for Scientific Research (B; No. 16H03179 to H.C.), and the University of Connecticut (to M.D.S.).

REFERENCES

(1) Jain, R. K.; Stylianopoulos, T. Delivering Nanomedicine to Solid Tumors. *Nat. Rev. Clin. Oncol.* **2010**, *7*, 653−664.

(2) Golombek, S. K.; May, J.-N.; Theek, B.; Appold, L.; Drude, N.; Kiessling, F.; Lammers, T. Tumor Targeting *Via* Epr: Strategies to Enhance Patient Responses. *Adv. Drug Delivery Rev.* **2018**, *130*, 17−38.

DOI: 10.1021/acsnano.8b07865
ACS Nano 2019, 13, 6396−6408

(3) Nel, A.; Ruoslahti, E.; Meng, H. New Insights into "Permeability" as in the Enhanced Permeability and Retention Effect of Cancer Nanotherapeutics. *ACS Nano* **2017**, *11*, 9567−9569.
(4) Lee, H.; Shields, A. F.; Siegel, B. A.; Miller, K. D.; Krop, I.; Ma, C. X.; LoRusso, P. M.; Munster, P. N.; Campbell, K.; Gaddy, D. F.; et al. 64cu-Mm-302 Positron Emission Tomography Quantifies Variability of Enhanced Permeability and Retention of Nanoparticles in Relation to Treatment Response in Patients with Metastatic Breast Cancer. *Clin. Cancer Res.* **2017**, *23*, 4190−4202.
(5) Stylianopoulos, T.; Munn, L. L.; Jain, R. K. Reengineering the Physical Microenvironment of Tumors to Improve Drug Delivery and Efficacy: From Mathematical Modeling to Bench to Bedside. *Trends Cancer* **2018**, *4*, 292−319.
(6) Cabral, H.; Matsumoto, Y.; Mizuno, K.; Chen, Q.; Murakami, M.; Kimura, M.; Terada, Y.; Kano, M. R.; Miyazono, K.; Uesaka, M.; Nishiyama, N.; Kataoka, K. Accumulation of Sub-100 Nm Polymeric Micelles in Poorly Permeable Tumours Depends on Size. *Nat. Nanotechnol.* **2011**, *6*, 815−823.
(7) Stylianopoulos, T.; Martin, J. D.; Chauhan, V. P.; Jain, S. R.; Diop-Frimpong, B.; Bardeesy, N.; Smith, B. L.; Ferrone, C. R.; Hornicek, F. J.; Boucher, Y.; Munn, L. L.; Jain, R. K. Causes, Consequences, and Remedies for Growth-Induced Solid Stress in Murine and Human Tumors. *Proc. Natl. Acad. Sci. U. S. A.* **2012**, *109*, 15101−15108.
(8) Stylianopoulos, T.; Jain, R. K. Combining Two Strategies to Improve Perfusion and Drug Delivery in Solid Tumors. *Proc. Natl. Acad. Sci. U. S. A.* **2013**, *110*, 18632−18637.
(9) Jiang, W.; Huang, Y.; An, Y.; Kim, B. Y. Remodeling Tumor Vasculature to Enhance Delivery of Intermediate-Sized Nanoparticles. *ACS Nano* **2015**, *9*, 8689−8696.
(10) Chauhan, V. P.; Stylianopoulos, T.; Martin, J. D.; Popovic, Z.; Chen, O.; Kamoun, W. S.; Bawendi, M. G.; Fukumura, D.; Jain, R. K. Normalization of Tumour Blood Vessels Improves the Delivery of Nanomedicines in a Size-Dependent Manner. *Nat. Nanotechnol.* **2012**, *7*, 383−388.
(11) Chauhan, V. P.; Martin, J. D.; Liu, H.; Lacorre, D. A.; Jain, S. R.; Kozin, S. V.; Stylianopoulos, T.; Mousa, A. S.; Han, X.; Adstamongkonkul, P.; Popovic, Z.; Huang, P.; Bawendi, M. G.; Boucher, Y.; Jain, R. K. Angiotensin Inhibition Enhances Drug Delivery and Potentiates Chemotherapy by Decompressing Tumour Blood Vessels. *Nat. Commun.* **2013**, *4*, 2516.
(12) Papageorgis, P.; Polydorou, C.; Mpekris, F.; Voutouri, C.; Agathokleous, E.; Kapnissi-Christodoulou, C. P.; Stylianopoulos, T. Tranilast-Induced Stress Alleviation in Solid Tumors Improves the Efficacy of Chemo-and Nanotherapeutics in a Size-Independent Manner. *Sci. Rep.* **2017**, *7*, 46140.
(13) Subbiah, V.; Grilley-Olson, J. E.; Combest, A.; Sharma, N.; Tran, R. H.; Bobe, I.; Osada, A.; Takahashi, K.; Balkissoon, J.; Camp, A.; et al. Phase 1b/2 Trial of Nc-6004 (Nanoparticle Cisplatin) Plus Gemcitabine in Patients with Advanced Solid Tumors. *Clin. Cancer Res.* **2018**, *24*, 43−51.
(14) Goel, S.; Duda, D. G.; Xu, L.; Munn, L. L.; Boucher, Y.; Fukumura, D.; Jain, R. K. Normalization of the Vasculature for Treatment of Cancer and Other Diseases. *Physiol. Rev.* **2011**, *91*, 1071−1121.
(15) Heiss, J. D.; Papavassiliou, E.; Merrill, M. J.; Nieman, L.; Knightly, J. J.; Walbridge, S.; Edwards, N. A.; Oldfield, E. H. Mechanism of Dexamethasone Suppression of Brain Tumor-Associated Vascular Permeability in Rats. Involvement of the Glucocorticoid Receptor and Vascular Permeability Factor. *J. Clin. Invest.* **1996**, *98*, 1400−1408.
(16) Wang, H.; Wang, Y.; Rayburn, E. R.; Hill, D. L.; Rinehart, J. J.; Zhang, R. Dexamethasone as a Chemosensitizer for Breast Cancer Chemotherapy: Potentiation of the Antitumor Activity of Adriamycin, Modulation of Cytokine Expression, and Pharmacokinetics. *Int. J. Oncol.* **2007**, *30*, 947−953.
(17) Kristjansen, P. E.; Boucher, Y.; Jain, R. K. Dexamethasone Reduces the Interstitial Fluid Pressure in a Human Colon Adenocarcinoma Xenograft. *Cancer Res.* **1993**, *53*, 4764−4766.
(18) Tolaney, S. M.; Boucher, Y.; Duda, D. G.; Martin, J. D.; Seano, G.; Ancukiewicz, M.; Barry, W. T.; Goel, S.; Lahdenrata, J.; Isakoff, S. J.; et al. Role of Vascular Density and Normalization in Response to Neoadjuvant Bevacizumab and Chemotherapy in Breast Cancer Patients. *Proc. Natl. Acad. Sci. U. S. A.* **2015**, *112*, 14325−14330.
(19) Polydorou, C.; Mpekris, F.; Papageorgis, P.; Voutouri, C.; Stylianopoulos, T. Pirfenidone Normalizes the Tumor Microenvironment to Improve Chemotherapy. *Oncotarget* **2017**, *8*, 24506−24517.
(20) Tong, R. T.; Boucher, Y.; Kozin, S. V.; Winkler, F.; Hicklin, D. J.; Jain, R. K. Vascular Normalization by Vascular Endothelial Growth Factor Receptor 2 Blockade Induces a Pressure Gradient across the Vasculature and Improves Drug Penetration in Tumors. *Cancer Res.* **2004**, *64*, 3731−3736.
(21) Baish, J. W.; Stylianopoulos, T.; Lanning, R. M.; Kamoun, W. S.; Fukumura, D.; Munn, L. L.; Jain, R. K. Scaling Rules for Diffusive Drug Delivery in Tumor and Normal Tissues. *Proc. Natl. Acad. Sci. U. S. A.* **2011**, *108*, 1799−803.
(22) Baxter, L. T.; Jain, R. K. Transport of Fluid and Macromolecules in Tumors. I. Role of Interstitial Pressure and Convection. *Microvasc. Res.* **1989**, *37*, 77−104.
(23) Baxter, L. T.; Jain, R. K. Transport of Fluid and Macromolecules in Tumors. Ii. Role of Heterogeneous Perfusion and Lymphatics. *Microvasc. Res.* **1990**, *40*, 246−263.
(24) Baxter, L. T.; Jain, R. K. Transport of Fluid and Macromolecules in Tumors. Iii. Role of Binding and Metabolism. *Microvasc. Res.* **1991**, *41*, 5−23.
(25) Baxter, L. T.; Jain, R. K. Transport of Fluid and Macromolecules in Tumors. Iv. A Microscopic Model of the Perivascular Distribution. *Microvasc. Res.* **1991**, *41*, 252−272.
(26) Mochida, Y.; Cabral, H.; Miura, Y.; Albertini, F.; Fukushima, S.; Osada, K.; Nishiyama, N.; Kataoka, K. Bundled Assembly of Helical Nanostructures in Polymeric Micelles Loaded with Platinum Drugs Enhancing Therapeutic Efficiency against Pancreatic Tumor. *ACS Nano* **2014**, *8*, 6724−6738.
(27) Nishiyama, N.; Okazaki, S.; Cabral, H.; Miyamoto, M.; Kato, Y.; Sugiyama, Y.; Nishio, K.; Matsumura, Y.; Kataoka, K. Novel Cisplatin-Incorporated Polymeric Micelles Can Eradicate Solid Tumors in Mice. *Cancer Res.* **2003**, *63*, 8977−8983.
(28) Fang, L.; He, Y.; Tong, Y.; Hu, L.; Xin, W.; Liu, Y.; Zhong, L.; Zhang, Y.; Huang, P. Flattened Microvessel Independently Predicts Poor Prognosis of Patients with Non-Small Cell Lung Cancer. *Oncotarget* **2017**, *8*, 30092−30099.
(29) Padera, T. P.; Stoll, B. R.; Tooredman, J. B.; Capen, D.; di Tomaso, E.; Jain, R. K. Pathology: Cancer Cells Compress Intratumour Vessels. *Nature* **2004**, *427*, 695.
(30) Smith, N. R.; Baker, D.; Farren, M.; Pommier, A.; Swann, R.; Wang, X.; Mistry, S.; McDaid, K.; Kendrew, J.; Womack, C.; et al. Tumor Stromal Architecture Can Define the Intrinsic Tumor Response to Vegf-Targeted Therapy. *Clin. Cancer Res.* **2013**, *19*, 6943−6956.
(31) Miao, L.; Liu, Q.; Lin, C. M.; Luo, C.; Wang, Y.; Liu, L.; Yin, W.; Hu, S.; Kim, W. Y.; Huang, L. Targeting Tumor-Associated Fibroblasts for Therapeutic Delivery in Desmoplastic Tumors. *Cancer Res.* **2017**, *77*, 719−731.
(32) Bridgeman, V. L.; Vermeulen, P. B.; Foo, S.; Bilecz, A.; Daley, F.; Kostaras, E.; Nathan, M. R.; Wan, E.; Frentzas, S.; Schweiger, T.; et al. Vessel Co-Option Is Common in Human Lung Metastases and Mediates Resistance to Anti-Angiogenic Therapy in Preclinical Lung Metastasis Models. *J. Pathol.* **2017**, *241*, 362−374.
(33) Wang, H.; Li, M.; Rinehart, J. J.; Zhang, R. Pretreatment with Dexamethasone Increases Antitumor Activity of Carboplatin and Gemcitabine in Mice Bearing Human Cancer Xenografts: *In Vivo* Activity, Pharmacokinetics, and Clinical Implications for Cancer Chemotherapy. *Clin. Cancer Res.* **2004**, *10*, 1633−1644.
(34) Li, Z.; Dong, J.; Zou, T.; Du, C.; Li, S.; Chen, C.; Liu, R.; Wang, K. Dexamethasone Induces Docetaxel and Cisplatin Resistance Partially through Up-Regulating Krüppel-Like Factor 5 in Triple-Negative Breast Cancer. *Oncotarget* **2017**, *8*, 11555−11565.
(35) Leggas, M.; Kuo, K.-L.; Robert, F.; Cloud, G.; deShazo, M.; Zhang, R.; Li, M.; Wang, H.; Davidson, S.; Rinehart, J. Intensive Anti-Inflammatory Therapy with Dexamethasone in Patients with Non-

DOI: 10.1021/acsnano.8b07865
ACS Nano 2019, 13, 6396−6408

Small Cell Lung Cancer: Effect on Chemotherapy Toxicity and Efficacy. *Cancer Chemother. Pharmacol.* **2009**, *63*, 731−743.
(36) Rinehart, J.; Keville, L.; Measel, J.; Spiekerman, A. M.; Burke, K. Corticosteroid Alteration of Carboplatin-Induced Hematopoietic Toxicity in a Murine Model. *Blood* **1995**, *86*, 4493−4499.
(37) Rinehart, J.; Keville, L.; Neidhart, J.; Wong, L.; DiNunno, L.; Kinney, P.; Aberle, M.; Tadlock, L.; Cloud, G. Hematopoietic Protection by Dexamethasone or Granulocyte-Macrophage Colony-Stimulating Factor (Gm-Csf) in Patients Treated with Carboplatin and Ifosfamide. *Am. J. Clin. Oncol.* **2003**, *26*, 448−458.
(38) Armitage, P. A.; Schwindack, C.; Bastin, M. E.; Whittle, I. R. Quantitative Assessment of Intracranial Tumor Response to Dexamethasone Using Diffusion, Perfusion and Permeability Magnetic Resonance Imaging. *Magn. Reson. Imaging* **2007**, *25*, 303−310.
(39) Sipos, B.; Kojima, M.; Tiemann, K.; Klapper, W.; Kruse, M. L.; Kalthoff, H.; Schniewind, B.; Tepel, J.; Weich, H.; Kerjaschki, D.; et al. Lymphatic Spread of Ductal Pancreatic Adenocarcinoma Is Independent of Lymphangiogenesis. *J. Pathol.* **2005**, *207*, 301−312.

DOI: 10.1021/acsnano.8b07865
ACS Nano 2019, 13, 6396−6408

Supplementary Materials

Dexamethasone Increases Cisplatin-Loaded Nanocarrier Delivery and Efficacy in Metastatic Breast Cancer by Normalizing the Tumor Microenvironment

John D. Martin[1], Myrofora Panagi[2], Chenyu Wang[3], Thahomina T. Khan[1], Margaret R. Martin[1], Chrysovalantis Voutouri[2], Kazuko Toh[4], Panagiotis Papageorgis[2,5], Fotios Mpekris[2], Christiana Polydorou[2], Genichiro Ishii[6], Shinichiro Takahashi[7], Naoto Gotohda[7], Toshiyuki Suzuki[7], Matthew E. Wilhelm[3], Vinicio Alejandro Melo[4], Sabina Quader[4], Jumpei Norimatsu[1], Ryan M. Lanning[8], Motohiro Kojima[6], Matthew David Stuber[3], Triantafyllos Stylianopoulos[2], Kazunori Kataoka[4,9*], and Horacio Cabral[1*]

Affiliations:

[1] *Department of Bioengineering, Graduate School of Engineering, The University of Tokyo, Bunkyo, Tokyo, 113-8656, Japan.*

[2] *Cancer Biophysics Laboratory, Department of Mechanical and Manufacturing Engineering, University of Cyprus, Nicosia, 1678, Cyprus.*

[3] *Process Systems and Operations Research Laboratory, Department of Chemical and Biomolecular Engineering, University of Connecticut, Storrs, Connecticut, 06269, USA.*

[4] *Innovation Center of NanoMedicine, Kawasaki Institute of Industrial Promotion, Kawasaki, Kanagawa, 210-0821, Japan.*

[5] *Department of Life Sciences, Program in Biological Sciences, European University Cyprus, Nicosia, 1516, Cyprus.*

[6] *Exploratory Oncology Research & Clinical Trial Center, National Cancer Center, Kashiwa, Chiba, 277-8577, Japan.*

[7] *Department of Hepatobiliary-Pancreatic Surgery, National Cancer Center Hospital East, Kashiwa, Chiba, 277-8577, Japan.*

[8] *Department of Radiation Oncology, School of Medicine, University of Colorado, Aurora, Colorado, 80045, USA.*

[9] *Institute for Future Initiatives, The University of Tokyo, Bunkyo, Tokyo, 113-0033, Japan.*

** Correspondence to: kataoka@ifi.t.u-tokyo.ac.jp (KK), horacio@bmw.t.u-tokyo.ac.jp (HC)*

Mathematical Model

Equations and assumptions: We used a 1-dimensional spherical tumor transport model. We assumed spatial independence for physiological parameters, which does not account for the heterogeneity of the tumor microenvironment (TME). Besides not considering vessels, cells and extracellular matrix (ECM) explicitly, we also assume a lack of lymphatics and nanocarrier (NC) binding. Lymphatics within tumors are largely non-functional. NCs are PEGylated to limit cellular interaction. Given our bolus injection mode of administration of probe and NC, we assume the source of fluid and NC is distributed continuously over the spatial domain and NC concentration decays exponentially.

The interstitial fluid transport follows Darcy's law and we assume axisymmetric flow:

$$\mathbf{u} = -K\nabla\mathbf{p}$$

where **u** is the interstitial fluid velocity (cm/s), *K* is the hydraulic conductivity of tumor interstitium (cm^2/mm Hg-sec), **p** is the interstitial fluid pressure (IFP) in mmHg.

We substituted the above equation into the fluid continuity equation to obtain the steady-state fluid transport model:

$$\nabla^2 p = \frac{SL_p}{VK}(p - p_{ss})$$

where L_p is the hydraulic conductivity of microvascular wall (cm/mmHg-sec), $\frac{S}{V}$ is the vascular surface area per unit volume (cm^{-1}), and p_{ss} is the steady-state interstitial pressure where the efflux from the vessels equals to the influx (mmHg).

The boundary conditions consist of the no-flux condition at the center of the spherical tumor and fixed tissue pressure p_∞ at the tumor edge (r=R):

$$\nabla p\big|_{r=0} = 0$$
$$p\big|_{r=R} = p_\infty$$

Solute transport follows the dynamic convection-diffusion equation below.

$$\frac{\partial C}{\partial t} + \nabla\cdot(\mathbf{u}C) = \nabla\cdot(D\nabla C) + \phi_s$$

where C is the concentration of the NC in the interstitium of the tumor (g/ml), D is the diffusion coefficient (cm^2/sec), and ϕ_s is the distributed source term based on the pore model for transcapillary exchange:

$$\phi_s = L_p \frac{S}{V}(p_v - p)(1-\sigma)C_v + P\frac{S}{V}(C_v - C)\frac{Pe}{e^{Pe}-1}$$

where p_v is the microvascular pressure (MVP) in mmHg; $Pe = L_p(p_v - p)(1 - \sigma)/P$ is the Peclet number representing the ratio of convective forces to diffusion forces across the vascular wall; σ is the solute reflection coefficient; P is the vascular permeability of the solute through the vascular wall (cm/sec); and C_v is the probe concentration in tumor vessels (g/ml). As described above, we assumed the vascular solute concentration decays exponentially with time:

$$C_v = C_o e^{-t/k_d}$$

where C_o is the initial probe concentration in the blood (g/ml), and k_d is the half-life circulation time of the probe (sec). The probe concentration satisfies the no-flux condition at the center and is continuous across the tumor periphery:

$$-D\frac{\partial C}{\partial r}\bigg|_{r=0} + uC\big|_{r=0} = 0$$

$$C\big|_{r=R} = C_\infty$$

We followed the pore theory[1] to describe NC transport through the walls of vessels. Assuming the vessels to be cylindrical, we can evaluate the hydraulic conductivity of the vessels L_p, the vascular permeability P, and the solute reflection coefficient σ with the following three equations:

$$L_p = \frac{\gamma r_o^2}{8\mu L}$$

$$P = \frac{\gamma H D_o}{L}$$

$$\sigma = 1 - W$$

where γ is the fraction of the surface area occupied by pores; r_o is the pore radius (nm); μ is the blood viscosity (mmHg-sec); L is the thickness of the vessel wall (μm); D_o is the diffusion coefficient of the NC in free solution at 37°C given by the Stokes-Einstein relationship; H and W are diffusive and convective hindrance factors, respectively, based on the size ratio of NC to pore[1,2]:

$$H = \frac{6\pi\Phi}{K_t}$$

$$W = \frac{\Phi(2-\Phi)K_s}{2K_t}$$

where Φ is the partitioning coefficient defined as the ratio of the average intrapore concentration to that in the bulk solution at equilibrium. When the interactions between the solutes and pore wall are purely steric, the partitioning coefficient is taken as $\Phi = (1-\lambda)^2$, where λ is the ratio of particle size to the pore size. K_t and K_s factors for the convective hindrance term W are defined as follows:

$$K_t = \frac{9}{4}\pi^2\sqrt{2}(1-\lambda)^{-5/2}\left[1+\sum_{k=1}^{2}a_k(1-\lambda)^k\right]+\sum_{k=0}^{4}a_{k+3}\lambda^k$$

$$K_s = \frac{9}{4}\pi^2\sqrt{2}(1-\lambda)^{-5/2}\left[1+\sum_{k=1}^{2}b_k(1-\lambda)^k\right]+\sum_{k=0}^{4}b_{k+3}\lambda^k$$

The corresponding coefficients a_k and b_k are listed in Supplementary Table M1.

Supplementary Table M1: Hydrodynamic Coefficients for the Cylindrical Pore Model

k	1	2	3	4	5	6	7
a_k	-73/60	77293/50400	-22.5083	-5.6117	-0.3363	-1.216	1.647
b_k	7/60	-2227/50400	4.0180	-3.9788	-1.9215	4.392	5.006

Solution strategy: We solved the fluid and solute transport model numerically using a discretized form. First, we reformulated the model into its dimensionless form. Then, the finite difference method was used to derive the discrete form of the fluid transport model with the upwind scheme employed for discretization of the solute transport model. We solved these equations using the variable-step 4th-order Runge-Kutta method.

The experimentally measured values of effective permeability P_{eff} were used to obtain the average probe concentration profiles C_{avg} over the interstitial space – which are taken as data points for the parameter estimation problem – utilizing the following spatially-averaged conservation equation:

$$\frac{dC_{avg}}{dt} = P_{eff}\frac{S}{V}(C_v - C_{avg})$$

To formulate the parameter estimation optimization problem, we seek to minimize the sum of squared error (SSE) between the average concentration of the transport model $C_{avg,mod}$ and data $C_{avg,data}$ over the experimental time span:

$$\min_{\mathbf{P}\in P_{aram}} \sum_{i=1}^{n} (C_{avg,mod}(t,\mathbf{P}) - C_{avg,data}(t))^2$$

Since we hypothesize dexamethasone affects the hydraulic conductivity of the vessel wall and the interstitial space, we chose L_p and K as the uncertain model parameters for estimation. For the other parameters, we used the literature values presented in Supplementary Table M2. Since the Peclet number can be very high at some parameter values, the problem can be very stiff. To obtain better local optimization results, we multistart *fmincon* in MATLAB (The MathWorks) with the interior-point solver and pick the results with the lowest objective function values. This approach, along with local analysis, provide a high-likelihood of obtaining near-global optimal results for the two-variable problem.

Supplementary Table M2: Physiological Parameter Values for Use in the Model

Parameter	Definition	Value	Reference
S/V (cm^{-1})	Vascular density	200	[3]
D (cm^2/sec)	Diffusion coefficient	2e-7 (13 nm);1.375e-7 (32 nm)	[4]
p_v (mm Hg)	Vascular pressure	25	[5]
k_d (min)	Blood circulation time	1480 (13 nm); 1278 (32nm)	[6]
μ (mm Hg-sec)	Blood viscosity	3e-5	[7]
L (μm)	Vessel wall thickness	5	[8]
γ	Fraction of pore area	1e-3	[9]

Results and analysis: The local optima are shown in Supplementary Table M3.

The model predictions of vessel wall pore diameter and interstitial hydraulic conductivity produced from effective permeability measurements are consistent with our other experimental data. Specifically, our model predicts both doses of dexamethasone raise the interstitial hydraulic conductivity to a similar level. This is expected based on the similar effects of both doses on collagen I (Fig. 2C) and hyaluronan (Fig. 2D) levels

measured histologically. Furthermore, our model predicts that, while 3 mg/kg dexamethasone reduces vessel pore diameter by only 10%, 30 mg/kg dexamethasone reduces vessel pore size by 45%. This model prediction is consistent with the notion that the higher dose produces a stronger anti-angiogenic effect. Specifically, we observe more vessel pruning (Fig. 1D,E) and a distribution of vessel diameters skewing towards diameters (Supplementary Fig. S3,4) with 30 mg/kg dexamethasone treatment.

Supplementary Table M3: Local Optimums for Parameter Estimation Results

Results	**70 kDa rhodamine**			**500 kDa FITC**		
Dose	**Control**	**3 mg/kg**	**30 mg/kg**	**Control**	**3 mg/kg**	**30 mg/kg**
P_{eff} (cm/sec)	9.60e-7	4.61e-6	2.80e-6	8.18e-7	4.30e-6	1.62e-6
L_p (cm/mm Hg-sec)	1.04e-6	1.49e-6	3.50e-7	8.67e-7	7.17e-7	2.81e-7
K (cm^2/mm Hg-sec)	2.33e-7	8.57e-7	1.56e-6	2.97e-7	1.63e-6	1.68e-6
IFP (mm Hg)	24.01	23.46	20.30	23.80	21.85	19.32
Pore diameter (nm)	223	267	130	204	185	116

Supplementary Figures and Tables

Supplementary Table 1 – Dose schedule (timing in the header) of the current study in mice (top row) compared to the doses of clinical trials of CDDP/m (NCT02043288) converted from human to mouse doses by body surface area (bottom row). The total dose of dexamethasone is in the right column.

Time relative to CDDP/m	-72 [Hours]	-48	-24	-12	-6	0	12	24	36	48	Total dose
Current study dose	3 [mg/kg]	3	3			3		*			12
CDDP/m (NC-6004) trial dose equivalent in mice				4.11 [mg/kg]	4.11		0.82	0.82	0.82	0.82	11.5

*If another cycle is initiated, 3mg/kg would be administered at this time to begin the next cycle.

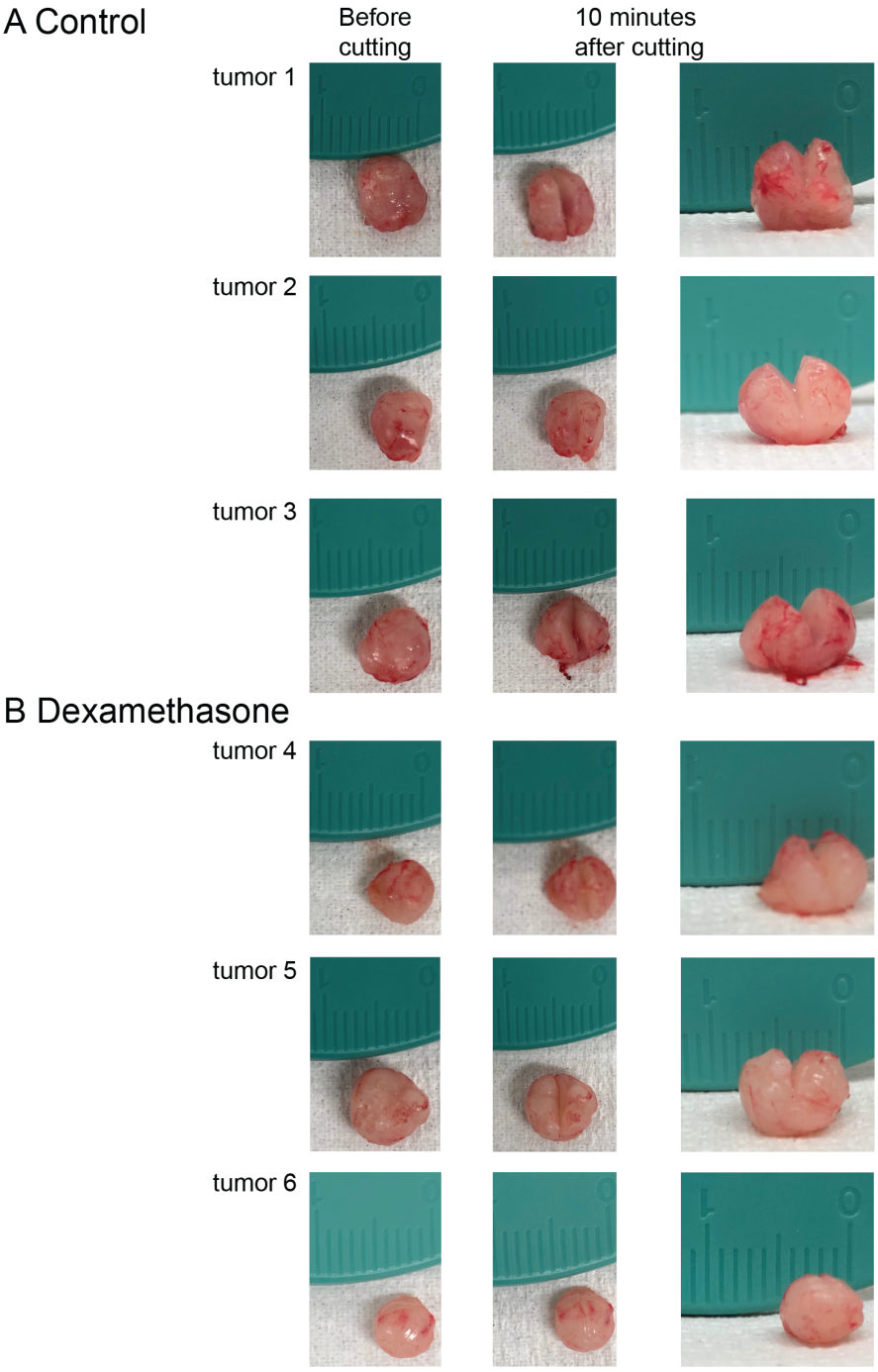

Supplementary Figure S1. Tumor opening assay. (**A-B**) Representative images of the tumor opening assay of 4T1 tumors from control (**A**) and 3mg/kg dexamethasone (**B**) treated mice. (**Left column**) Overhead images of the tumors before cutting. (**Center column**) Overhead images of the tumors after cutting. (**Right column**) *En face* images of the tumors after cutting. The tumor opening is the distance the tumor opens ten minutes after cutting. The larger the opening, the higher the solid stress in the tissues. Ruler scale in centimeters. These images were collected for representation and this data was not used in quantitation in Figure 2F.

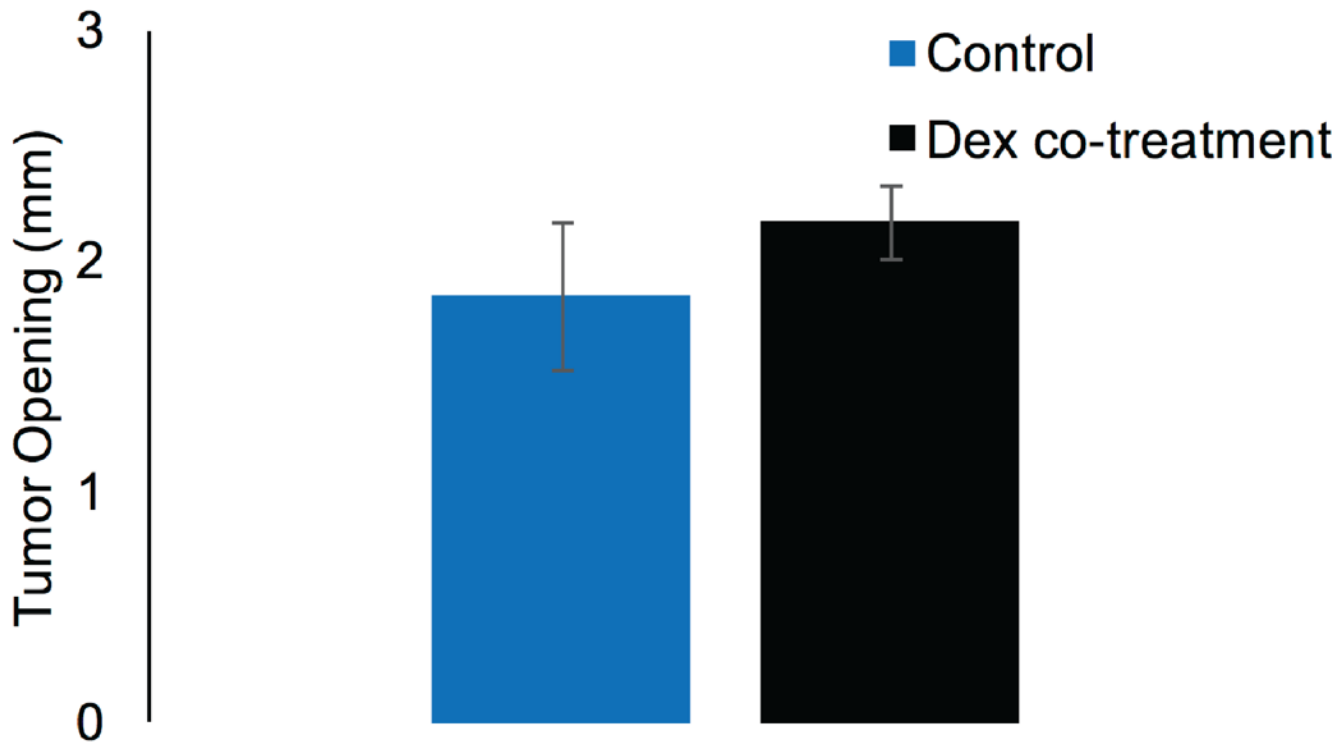

Supplementary Figure S2. Dexamethasone co-treatment does not affect solid stress. Quantification of the tumor opening distance, which is a measure of solid stress levels of 4T1 tumors excised from control mice (blue bar) or mice treated with 3 mg/kg dexamethasone 2 h before tumor excision and measurement (black bar, *N* = 3 mice per group).

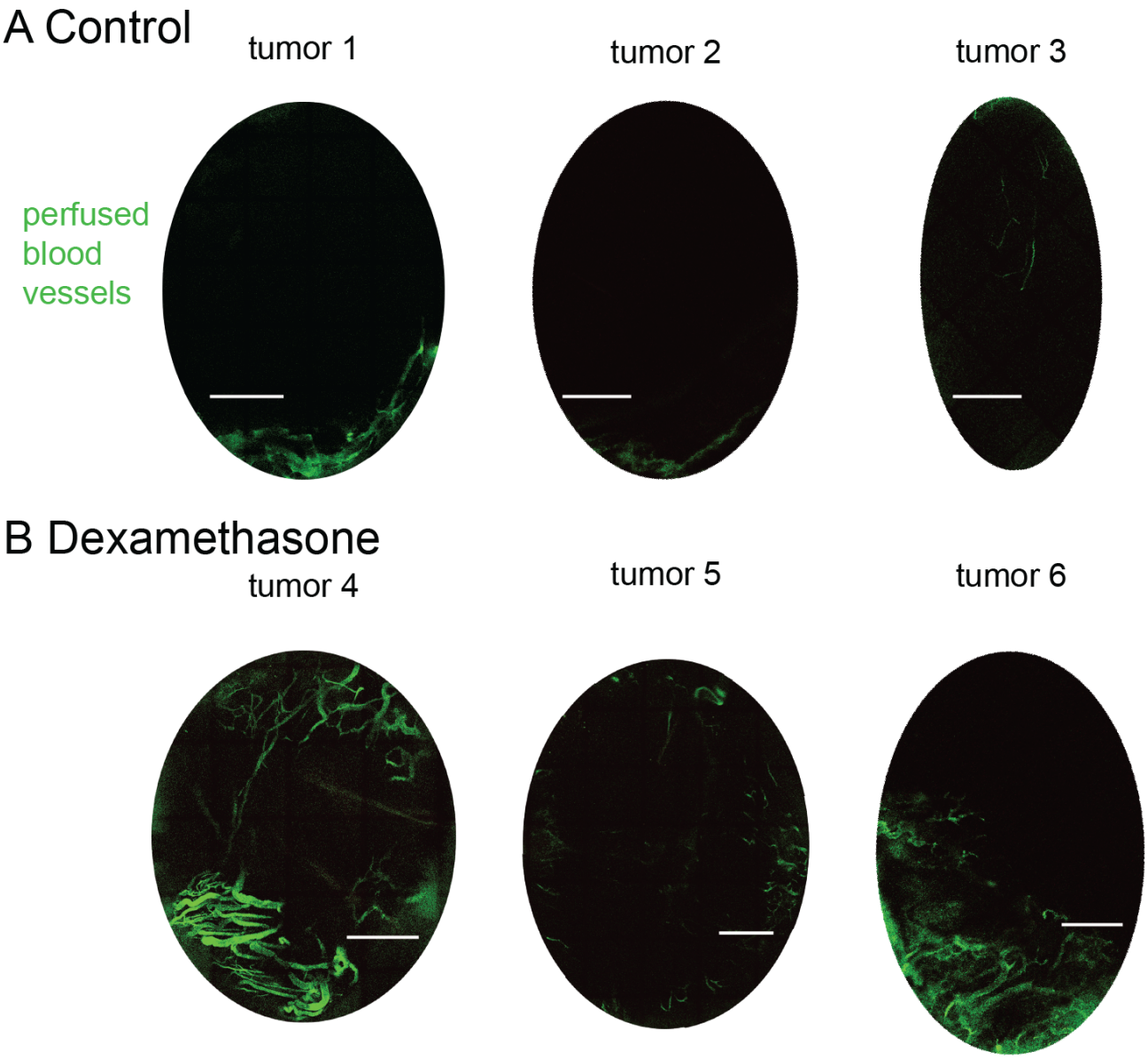

Supplementary Figure S3. Dexamethasone affects tumor vessel function. (**A-B**) Representative intravital microscopy images of perfused tumor vessels (green) of 4T1 tumors from control (**A**) and 3 mg/kg dexamethasone (**B**) treated mice. Scale bars = 600 μm.

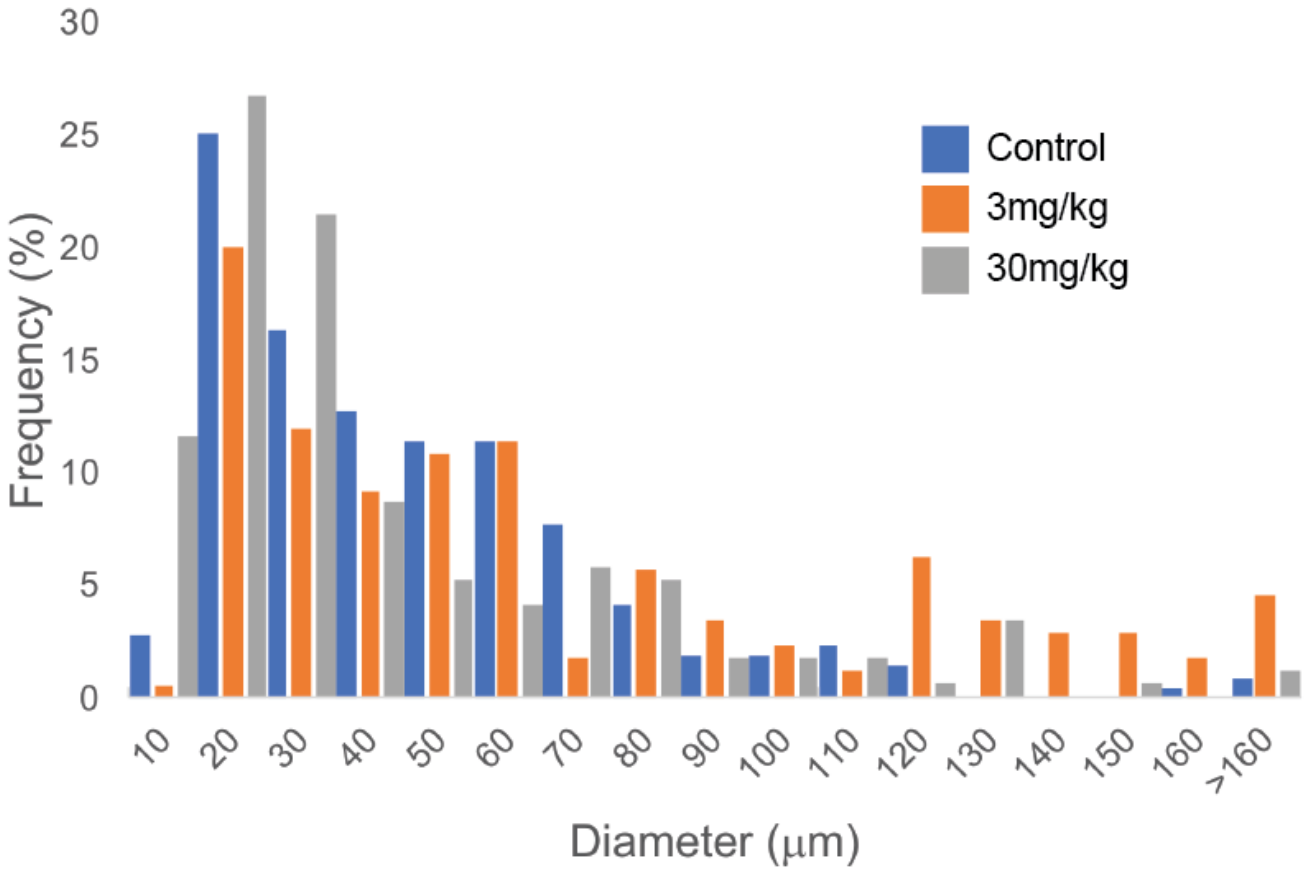

Supplementary Figure S4. Dexamethasone normalizes the diameter of vessels. Histograms of vessel diameters indicate a larger proportion of wider vessels with 3 mg/kg dexamethasone treatment (*N* = 3, n = 175-220 vessels per group).

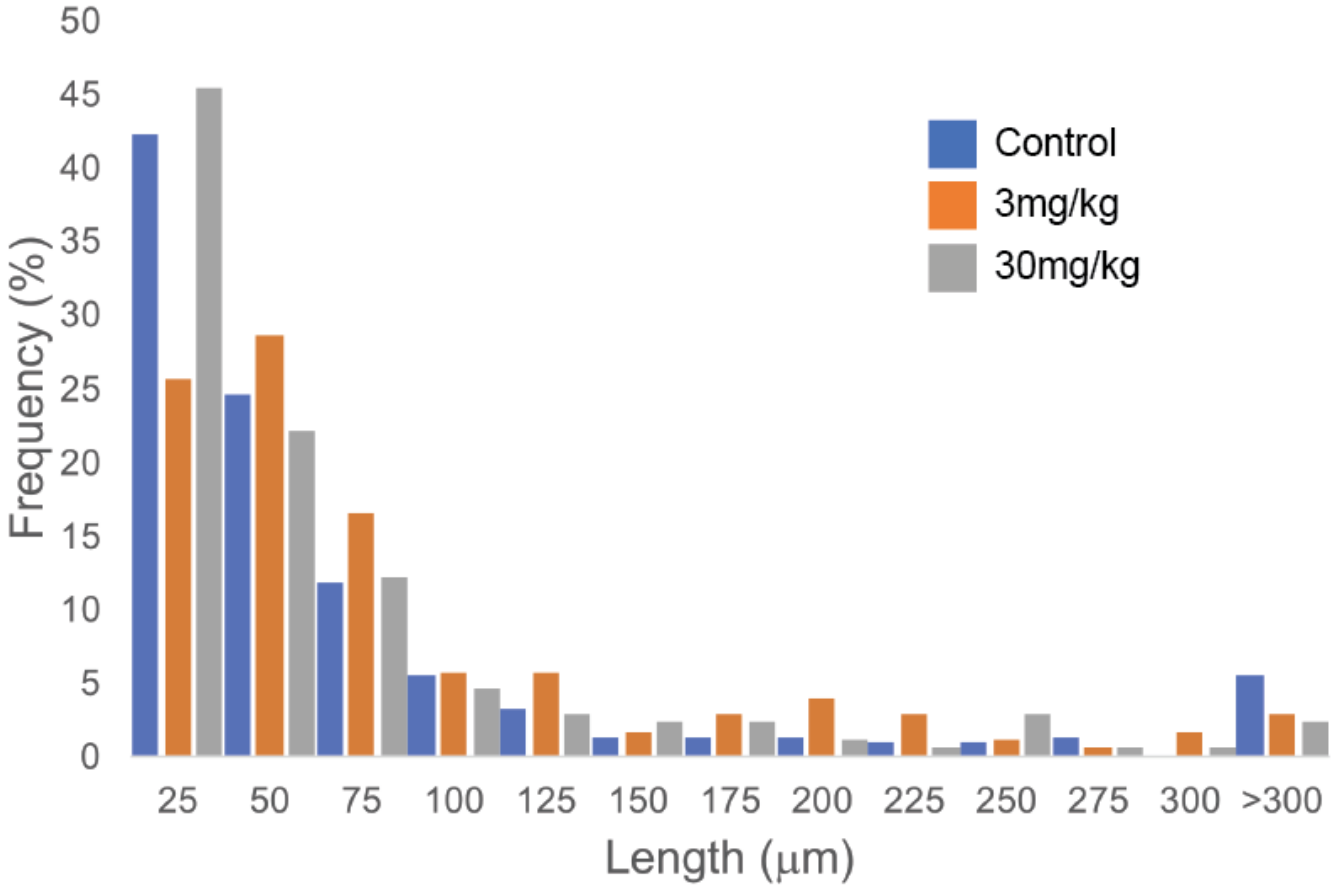

.

Supplementary Figure S5. Dexamethasone normalizes the length of vessels. Histograms of perfused vessel lengths from intravital microscopy indicate a larger proportion of longer vessels with 3 mg/kg dexamethasone treatment (*N* = 3 mice, n = 175-220 vessels per group).

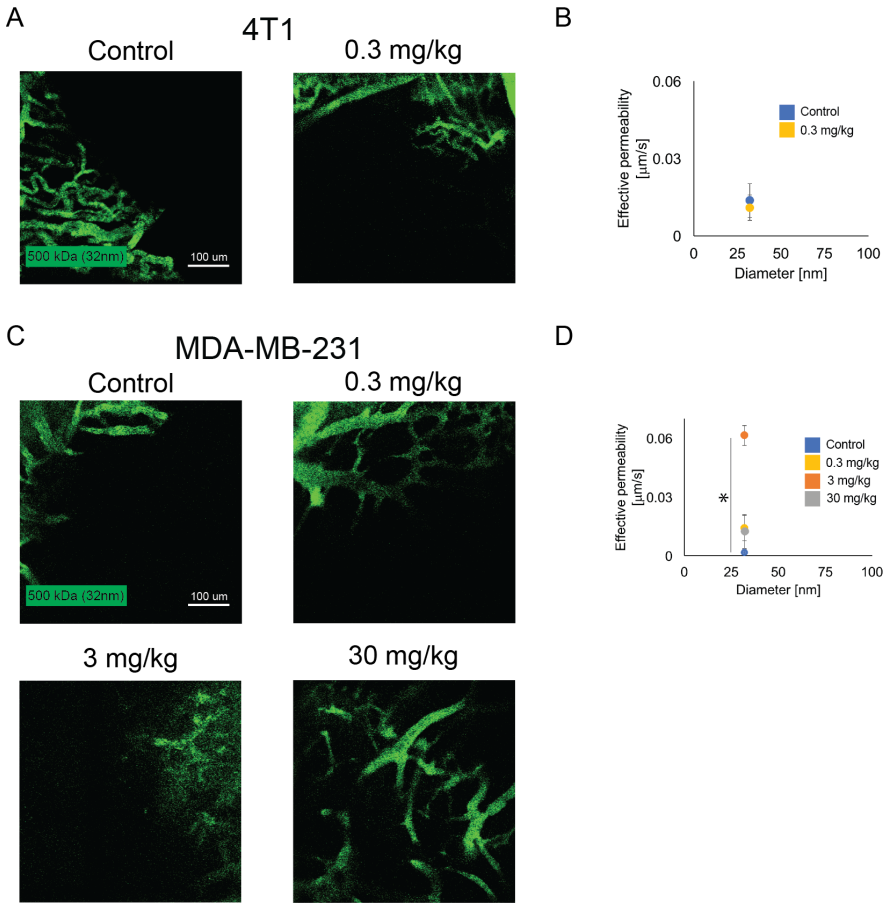

Supplementary Figure S6. Transvascular transport of nanocarriers after treatment of dexamethasone at various doses. Transvascular transport in 4T1 (**A, B**) and MDA-MB-231 (**C, D**) breast cancers, with (**A,C**) representative confocal intravital microscopy images of tumors. (**A**) 4T1 bearing mice were treated 4 days daily with (**left panel**) control or (**right panel**) 0.3 mg/kg dexamethasone, and the representative images show the distribution 20 min after injection of 500 kDa (32 nm, green) fluorescent dextrans. (**B**) Quantification of effective permeabilities, which is a measure of the rate that dextrans are transporting out of vessels and penetrating after treatment with 0.3 mg/kg dexamethasone (yellow circles) and control (blue circles) in mice bearing 4T1 breast tumors (*N* = 3). (**C**) MDA-MB-231 bearing mice were treated 4 days daily with (**top left panel**) control, (**top right panel**) 0.3 mg/kg, (**bottom left panel**) 3 mg/kg or (**bottomr right panel**) 30 mg/kg dexamethasone, and the representative images show the distribution 20 min after injection of 500 kDa (32 nm, green) fluorescent dextrans. (**D**) Quantification of effective permeabilities after treatment of 4 days daily dexamethasone at 0.3 mg/kg (yellow circles), 3 mg/kg (orange circles), 30 mg/kg (gray circles) and control (blue circles) doses in mice bearing MDA-MB-231 breast tumors (*N* = 3). Data expressed as mean ± standard error of the mean (*, P<0.05).

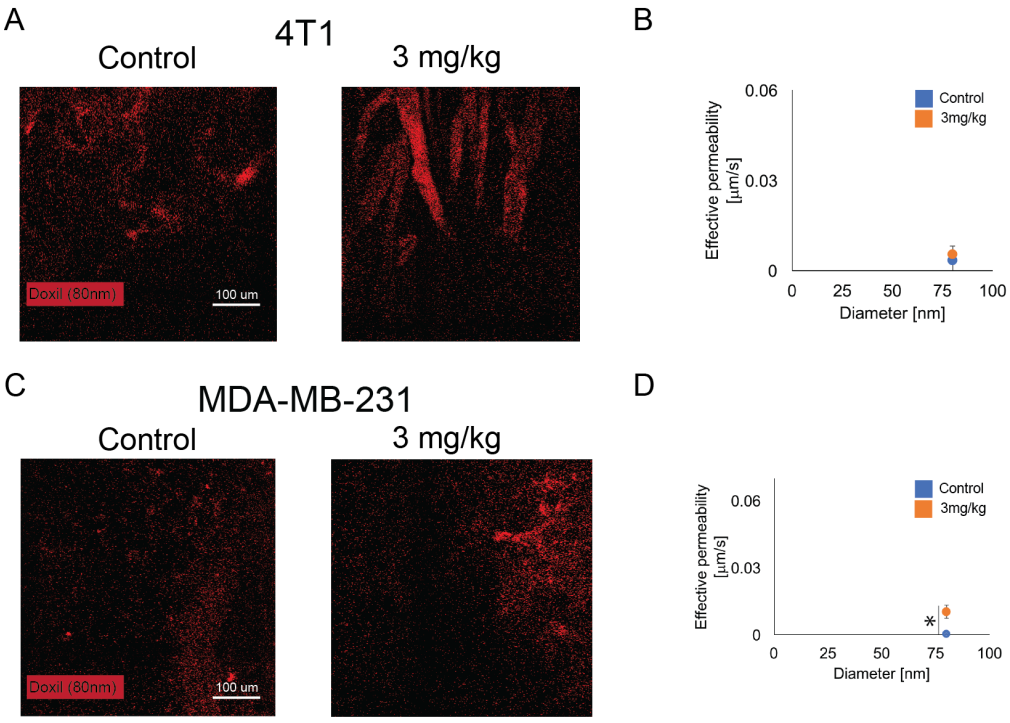

Supplementary Figure S7. Transvascular transport of Doxil after treatment of dexamethasone. Transvascular transport in 4T1 (**A, B**) and MDA-MB-231 (**C, D**) breast cancers, with (**A,C**) representative confocal intravital microscopy images of tumors. (**A**) 4T1 bearing mice were treated with (**left panel**) control or (**right panel**) 3 mg/kg dexamethasone, and the images show the distribution 20 min after injection of Doxil (80 nm, red). (**B**) Quantification of 4T1 effective permeabilities, which is a measure of the rate that Doxil is transporting out of vessels and penetrating after treatment of either 4 days daily dexamethasone 3 mg/kg (orange circles) or control (blue circles, *N* = 3). (**C**) MDA-MB-231 bearing mice were treated with (**left panel**) control or (**right panel**) 3 mg/kg dexamethasone, and the images show the distribution 20 min after injection of Doxil (80 nm, red). (**D**) Quantification of MDA-MB-231 effective permeabilities after treatment of either 4 days daily dexamethasone 3 mg/kg (orange circles) or control (blue circles, *N* = 3). Data expressed as mean ± standard error of the mean (*, P<0.05).

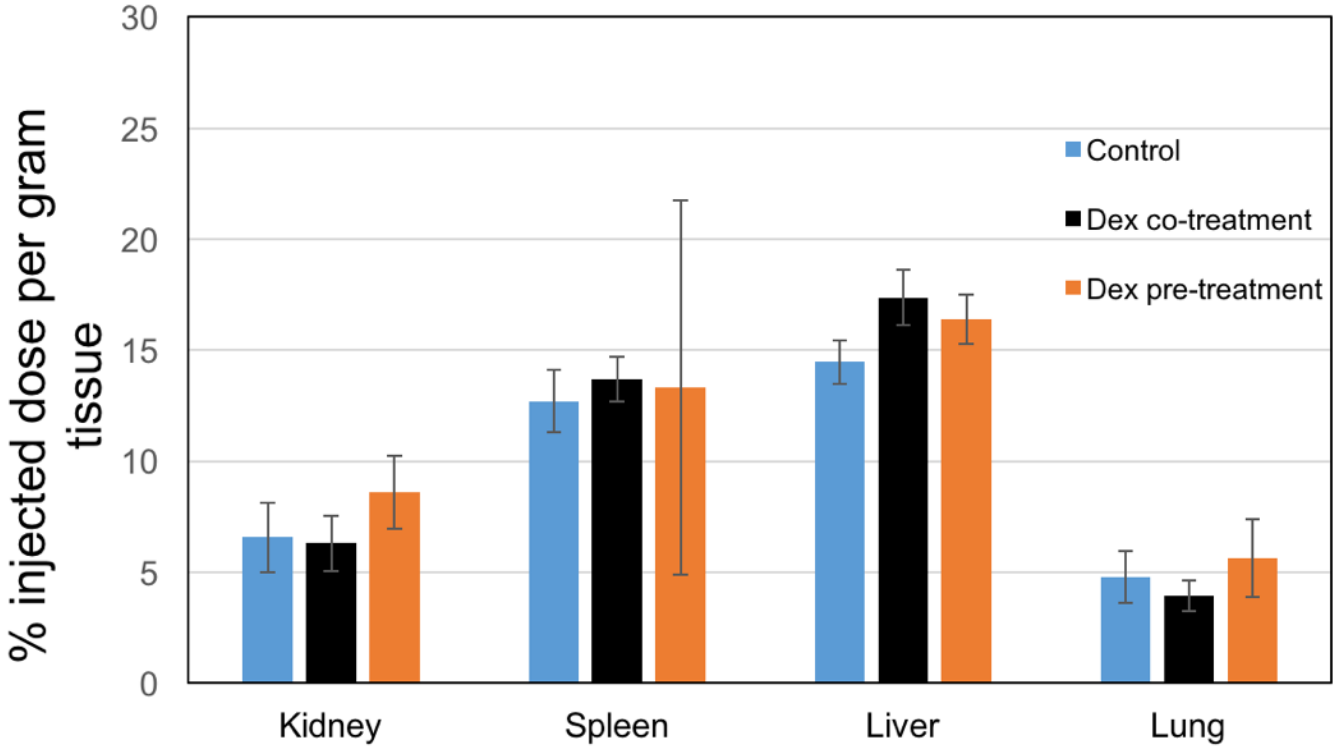

Supplementary Figure S8. Tissue distribution of CDDP/m with and without dexamethasone in major organs 24 h after CDDP/m administration. CDDP/m (5.5 mg/kg) was administered to 4T1 bearing mice (*N* = 6 per group) 2 h after the final dose of daily 3 mg/kg dexamethasone pre-treatment (orange bars) or a single dose of 3 mg/kg dexamethasone as a "co-treatment" (black bars). All data expressed as mean ± standard error of the mean.

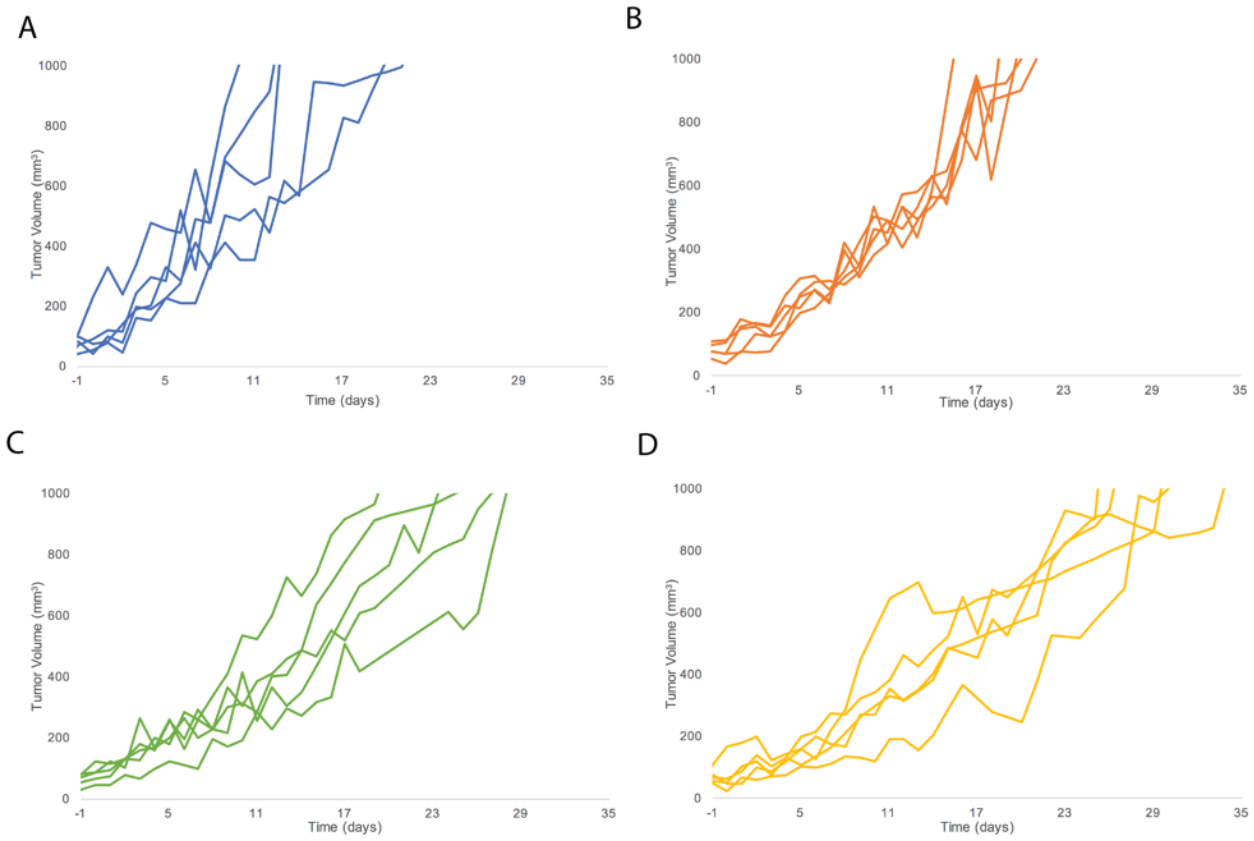

Supplementary Figure S9. Dexamethasone increases the efficacy of 30nm CDDP/m in primary breast cancer. (**A-D**) Tumor growth delay study in a syngeneic, orthotopic 4T1 breast tumor model treated with dexamethasone, CDDP/m, or the combination (*N* = 6). (**A**) Saline (control) treated mice tumors (blue) took an average of 3.2 days for the tumor volume to double and 17 days to reach 1000 cubic millimeters. (**B**) Dexamethasone treated mice tumors (orange) took 3.0 days for the tumor volume to double and 20 days to reach 1000 cubic millimeters. (**C**) CDDP/m treated mice tumors (green) took 3.8 days for the tumor volume to double and 24 days to reach 1000 cubic millimeters. (**D**) Dexamethasone and CDDP/m combination treated mice tumors (yellow) took 5.0 days for the tumor volume to double and 28 days to reach 1000 cubic millimeters.

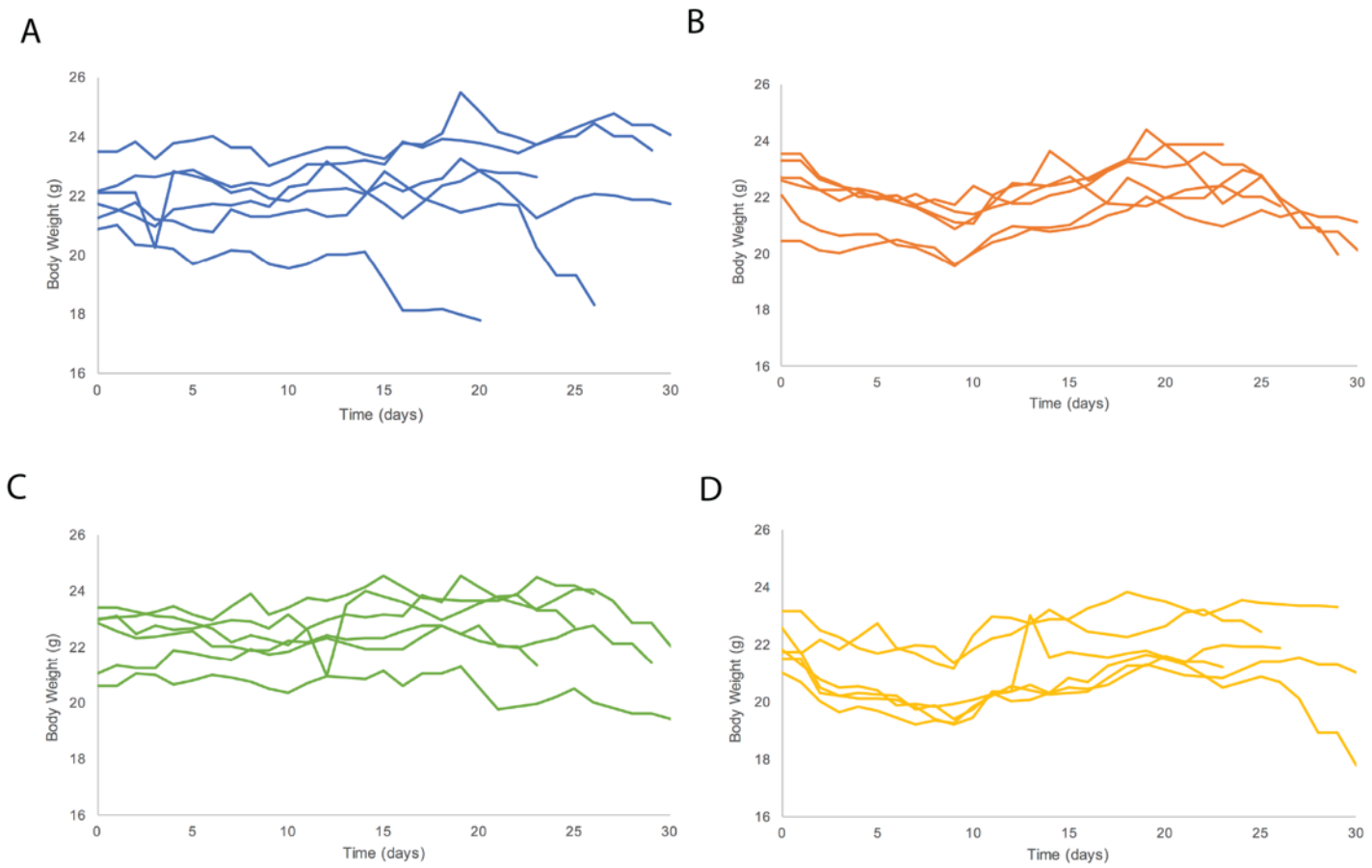

Supplementary Figure S10. Mouse body weight during the dexamethasone and 30nm CDDP/m tumor growth study in primary breast cancer. (**A-D**) Individual body weights measured during the tumor growth delay study in a syngeneic, orthotopic 4T1 breast tumor model treated with dexamethasone, CDDP/m, or the combination (*N* = 6). (**A**) Saline (control) treated mice (blue) lost weight earliest before morbidity. (**B**) Dexamethasone treated mice tumors (orange) seemed to lose weight after the initial period of treatment and associated with morbidity towards the end of the study. (**C**) CDDP/m treated mice tumors (green) seemed to lose weight only associated with morbidity towards the end of the study. (**D**) Dexamethasone and CDDP/m combination treated mice tumors (yellow) seemed to lose weight after the initial period of treatment but mostly retained their weight towards the end of the study.

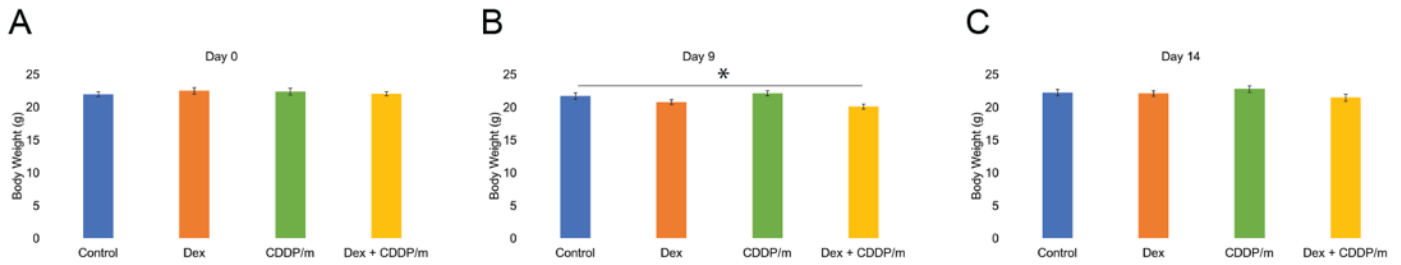

Supplementary Figure S11. The combination of dexamethasone and CDDP/m induces limited weight loss immediately following the treatment regimen. (**A-C**) Average mouse weights from the tumor growth delay study at various days in syngeneic, orthotopic 4T1 breast tumors treated with dexamethasone, CDDP/m, or the combination (*N* = 6). (**A**) All treatment groups started with the same body weight pre-treatment. (**B**) Combination treated mice had significantly lower body weight than the controls on the day 9, which was the conclusion of therapy (*P* = 0.03). (**C**) Combination treated mice did not have different weights than the control on day 14, which was 5 days after the conclusion of treatment. All data expressed as mean ± standard error of the mean (*, P < 0.05).

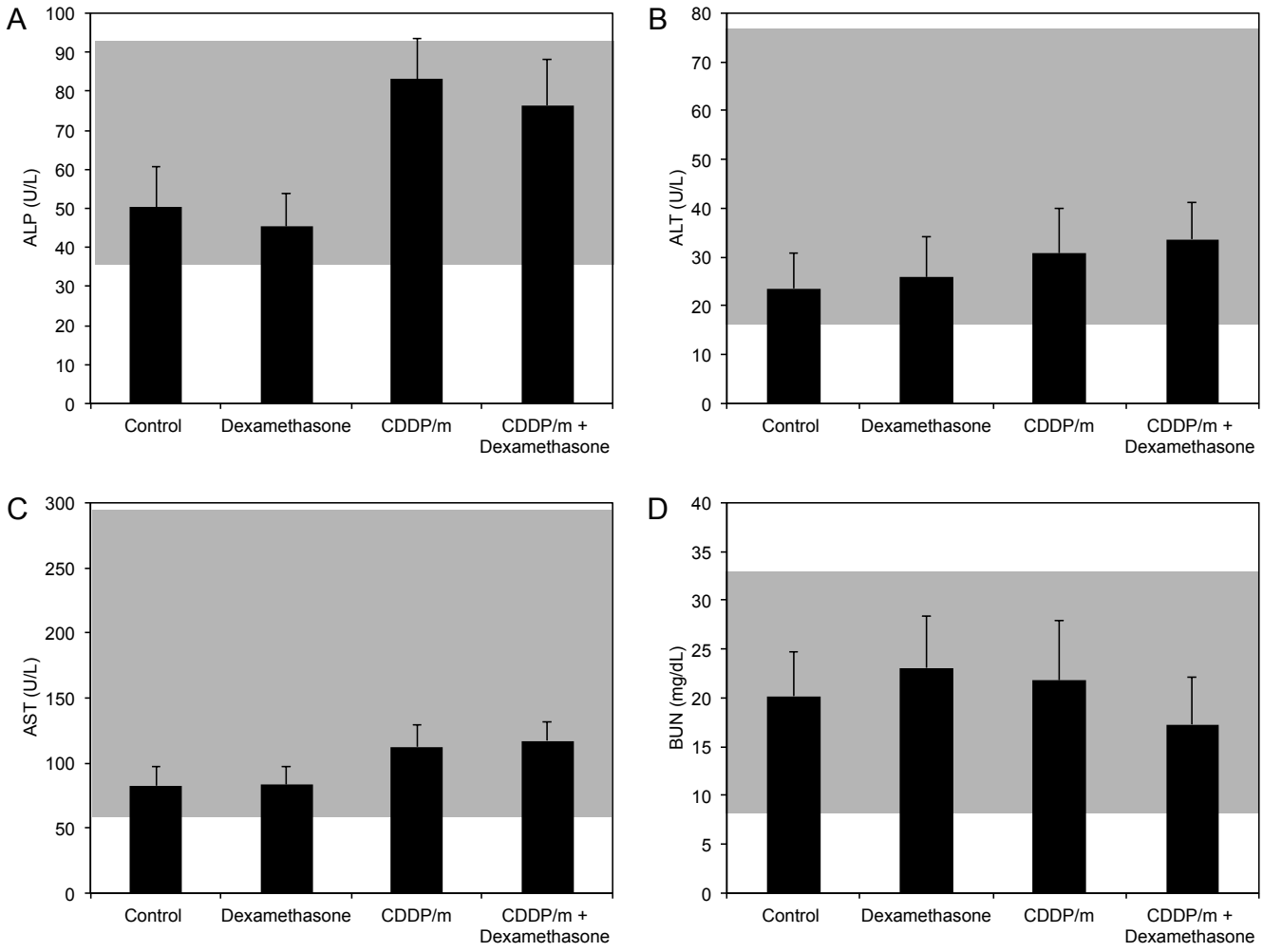

Supplementary Figure S12. Serum biochemistry of the mice after the treatments. Serum was collected from all mice after the final mouse reached the endpoint of the primary tumor efficacy study and serum biochemistry was assessed (n = 4). (**A-D**) Averages of serum biochemistry within each treatment group. (**A**) ALP, alkaline phosphatase. (**B**) ALT, alanine aminotransferase; (**C**) AST, aspartate aminotransferase. (**D**) BUN, blood urine nitrogen. Gray areas indicate the normal ranges for the markers. All data expressed as mean ± standard error of the mean.

Supplementary References

1. Bungay, P. M.; Brenner, H., The Motion of a Closely-Fitting Sphere in a Fluid-Filled Tube. *Int. J. Multiphase Flow* **1973,** *1*, 25-56.
2. Deen, W., Hindered Transport of Large Molecules in Liquid‐Filled Pores. *AIChE J.* **1987,** *33*, 1409-1425.
3. Yuan, F.; Salehi, H. A.; Boucher, Y.; Vasthare, U. S.; Tuma, R. F.; Jain, R. K., Vascular Permeability and Microcirculation of Gliomas and Mammary Carcinomas Transplanted in Rat and Mouse Cranial Windows. *Cancer Res* **1994,** *54*, 4564-4568.
4. Pluen, A.; Boucher, Y.; Ramanujan, S.; McKee, T. D.; Gohongi, T.; di Tomaso, E.; Brown, E. B.; Izumi, Y.; Campbell, R. B.; Berk, D. A.; Jain, R. K., Role of Tumor-Host Interactions in Interstitial Diffusion of Macromolecules: Cranial Vs. Subcutaneous Tumors. *Proc. Natl. Acad. Sci. U. S. A.* **2001,** *98*, 4628-4633.
5. Boucher, Y.; Jain, R. K., Microvascular Pressure Is the Principal Driving Force for Interstitial Hypertension in Solid Tumors: Implications for Vascular Collapse. *Cancer Res.* **1992,** *52*, 5110-5114.
6. Popović, Z.; Liu, W.; Chauhan, V. P.; Lee, J.; Wong, C.; Greytak, A. B.; Insin, N.; Nocera, D. G.; Fukumura, D.; Jain, R. K., A Nanoparticle Size Series for in Vivo Fluorescence Imaging. *Angew. Chem.* **2010,** *122*, 8831-8834.
7. Baish, J. W.; Netti, P. A.; Jain, R. K., Transmural Coupling of Fluid Flow in Microcirculatory Network and Interstitium in Tumors. *Microvasc Res* **1997,** *53*, 128-141.
8. Jain, R. K., Transport of Molecules across Tumor Vasculature. *Cancer Metastasis Rev.* **1987,** *6*, 559-593.
9. Chauhan, V. P.; Stylianopoulos, T.; Martin, J. D.; Popovic, Z.; Chen, O.; Kamoun, W. S.; Bawendi, M. G.; Fukumura, D.; Jain, R. K., Normalization of Tumour Blood Vessels Improves the Delivery of Nanomedicines in a Size-Dependent Manner. *Nat Nanotechnol* **2012,** *7*, 383-388.